



NTNU – Trondheim
Norwegian University of
Science and Technology

Modeling the propagation of streamers in liquids

The Townsend-Meek criterion and a novel model for photoionization

Inge Madshaven

Master of Science in Physics and Mathematics

Submission date: June 2015

Supervisor: Jon Andreas Støvneng, IFY

Norwegian University of Science and Technology
Department of Physics

Summary

Conducting channels form when a dielectric liquid is subjected to high electrical stress. These channels are known as streamers, and if allowed the time to form and propagate, they can lead to an electrical breakdown in the liquid. SINTEF has developed a numerical model for the propagation of streamers in liquids, which is based on the Townsend–Meek criterion, and is focused on impact ionization by electrons accelerated in an electric field.

The model is able to correctly predict many aspects of streamer propagation, but it predicts a propagation voltage that is too high, a degree of streamer branching that is somewhat low, and fails to replicate the transition to fast third and fourth mode streamers. In an attempt to improve the streamer model, the Townsend–Meek criterion and a novel model for photoionization is explored.

The most important parameter in the Townsend–Meek criterion is the Meek constant Q_c . This parameter describes the number of electrons required before an electron avalanche becomes unstable. Currently, $Q_c = 23$ is used by the model. This translates to an avalanche of 10^{10} electrons. Calculations done with data available in literature suggest that this value is too high, and that the definition used to calculate the Meek constant needs to be clarified.

The photoionization model assumes a high radiation peak from molecules relaxing from the lowest electronically excited state to the ground state. The radiation originates within the streamer channel head. The ionization rate is calculated by assuming an ionization cross section that is dependent on the magnitude of the electric field. A transition in speed is found when the electric field has reduced the ionization potential of the molecules to the energy of the lowest excited state.

Sammendrag

Elektrisk ledende kanaler dannes når en dielektrisk væske utsettes for høy elektrisk spenning. Disse kanalene er kjent som streamere, og hvis de gis tid til å forplante seg, kan de føre til elektrisk gjennomslag i væsken. SINTEF har utviklet en numerisk modell for forplantning av streamere i væsker. Modellen er basert på Townsend–Meek-kriteriet, og er fokusert på støttonisering utført av elektroner som blir akselerert i et elektrisk felt.

Modellen er i stand til å forutse mange viktige egenskaper til streamere, men spenningen som trengs for forplantning er for høy, graden av forgrening til streameren er noe lav, og modellen klarer ikke å gjenskape overgangen til hurtige tredje og fjerde modus streamere. I et forsøk på å forbedre streamermodellen blir Townsend–Meek-kriteriet og en ny modell for fotoionisering utforsket.

Den viktigste parameteren i Townsend–Meek-kriteriet er Meek-konstanten Q_c . Denne parameteren beskriver antall elektroner som kreves for at et elektronskred skal bli ustabil. Foreløpig brukes $Q_c = 23$ av modellen. Dette tilsvarer et skred på 10^{10} elektroner. Beregninger gjort på data tilgjengelig i litteratur tyder på at denne verdien er for høy, og at definisjonen som brukes til å beregne Meek-konstanten må avklares.


Modellen for fotoionisering antar en høy grad av stråling fra molekyler som relaxerer fra laveste eksiterte tilstand til grunntilstanden. Strålingen har opphav inne i tuppen på streameren. Ioniseringsraten beregnes ved å anta et ioniseringstverrsnitt som er avhengig av størrelsen på det elektriske feltet. En hastighetsovergang inntreffer når det elektriske feltet har redusert ioniseringspotensialet ned til energien til den laveste eksiterte tilstanden.

Preface

This master thesis is submitted to the Norwegian University of Science and Technology (NTNU), and marks the conclusion of a master's degree in applied physics. The work was performed at the institute of physics (IFY) with Jon Andreas Støvneng as supervisor, and was done in collaboration with Sintef, where Øystein Hestad was the main supervisor.

I would like to thank my supervisors Jon A. Støvneng and Øystein Hestad for allowing me to perform this work. I have received guidance and help from both Øystein Hestad and Torstein Grav at Sintef. I am also grateful towards both ABB and Hans Sverre Smalø for the inspiration to the photoionization model, and for fruitful discussions during the work.

All of my classmates have contributed to making my years at NTNU pleasant and interesting. In particular, I would like to acknowledge Trygve Sørgård and Jabir Ali Ouassou, for both casual and academical discussions, and for helping me proofread this thesis.


Inge Madshaven
Trondheim, June 18, 2015

Nomenclature

This is a list of the most used variables. Variables only used in a limited section are not necessarily repeated here, and are properly described where they are used. This list is sorted according to the sequence: numerals, Greek letter, then Roman letters, with capital letters first.

α	Townsend's first coefficient, avalanche parameter
α_{MAX}	Avalanche parameter, magnitude
β	Parameter for curve fitting field dependent IP
γ	Photon
$\Delta\lambda$	Width of the radiation peak
$\Delta\tau$	Model time step
ΔU	Energy difference
ϵ_0	Vacuum permittivity
ϵ_r	Relative permittivity
ϵ_1	First/lowest excitation energy
Θ	Maximum classically allowed angle
θ	Polar angle
θ_e	Angle of emitted electron
θ_γ	Angle between photon and electrical field
λ	Wavelength
λ_1	Wavelength corresponding to the first excitation energy
μ_e	Electron mobility
μ, ν, ϕ	Prolate spheroid coordinates
ν_0	Hyperbola defined by the needle
ρ	Density
σ_0	Maximum cross section

σ_{Ω}	Scaled angular cross section
σ_{ω}	Scaled energy dependent cross section
τ	Tunneling time
ω	Frequency
A	Neutral molecule
a	Distance between the plane and the focal of the hyperbola defined by the needle
B_p	Spectral radiance from a Planck distribution
B_g	Spectral radiance from a gauss peak
B_{g0}	Magnitude of spectral radiance from gauss peak
C	Constant given by the applied voltage and the gap parameters
C_{Ω}	Normalization constant for σ_{Ω}
d	Gap size/distance
E	Electrical field strength
E_0	Electrical field strength at the needle tip
E_{α}	Avalanche parameter, field strength scale
E_{a_0}	Electric field strength, 1 atomic unit
e^{-}	Electron
h	The Planck constant
\hbar	The reduced Planck constant
I	Ionization potential
k_{γ}	Photon momentum vector
k_B	The Boltzmann constant
ℓ	Length
m	Mass
N_{ε}	Number of excited molecules
N_0	Initial number of electrons
N_e	Number of electrons

N_I	Number of ionized molecules
Q_c	Meek constant, critical avalanche size, log scale
Q_i	Maximum avalanche size possible when initiating at a given position, log scale
Q_f	Maximum avalanche size possible at a given position, log scale
Q_{MAX}	Maximum avalanche size, log scale
r_0	Distance to the needle surface
r_p	Needle tip curvature radius
T	Temperature
U	Energy
V_0	Applied voltage
\mathcal{V}	Volume
v	Velocity
x, y, z	Cartesian coordinates

Contents

1	Introduction	1
1.1	Streamers in liquids	1
1.2	Dielectric breakdown	1
1.3	Research methods	2
1.4	Motivation	3
1.5	Scope and structure	4
2	Background theory	5
2.1	Streamers in liquids	5
2.1.1	Propagation modes	6
2.1.2	Propagation mechanisms	8
2.2	Ionization	10
2.2.1	Field ionization	11
2.2.2	Impact ionization	12
2.2.3	Photoionization	14
3	Numerical model	17
3.1	Geometry	17
3.2	The present numerical model	20
3.3	The Townsend–Meek criterion	22
3.4	Photoionization model	25
3.4.1	Photoionization in an electric field	25
3.4.2	Radiation	28
3.4.3	Ionization rate	31
3.4.4	Movement rate	32
3.4.5	Model parameters	33
4	Results	35
4.1	The Townsend–Meek criterion	35
4.1.1	Finding the Meek constant	36
4.1.2	Effect on the model	38
4.2	Photoionization model	40
4.2.1	Preliminaries	40

4.2.2	Spatial range	42
4.2.3	Voltage range	45
4.2.4	Movement rate	46
5	Discussion	49
5.1	The Townsend–Meek criterion	49
5.1.1	Defining the Meek constant from experiments	49
5.1.2	Defining a dynamic Meek constant	52
5.1.3	Effect on the model	53
5.2	Photoionization model	55
5.2.1	Cross section	55
5.2.2	Radiation and ionization	56
5.2.3	Movement rate	58
5.2.4	Potential seeds	59
5.3	Implementing photoionization	61
6	Conclusion	63
6.1	The Townsend–Meek criterion	63
6.2	Photoionization	64
A	Prolate spheroidal coordinates	67
A.1	Basic properties	67
A.2	Electrical properties	69
B	Calculations	71
C	Additional plots	75
C.1	The Townsend–Meek criterion	75
C.1.1	Finding the Meek constant	75
C.1.2	Effect on the model	78
C.2	Photoionization model	80
C.2.1	Preliminaries	80
C.2.2	Spatial range	82
C.2.3	Voltage range	86
C.2.4	Movement rate	90
	Bibliography	95

Chapter 1

Introduction

1.1 Streamers in liquids

The so-called streamers is the phenomenon given the most focus in the studies of dielectric breakdown in liquids.¹⁻⁹ The term streamer is, however, not well-defined, but it generally refers to a phenomenon that can be observed by Schlieren or shadowgraphic imaging techniques. These techniques exploit variations in the liquid's refractive index to create images.

A streamer is often described as a gaseous channel of weakly ionized plasma.⁴ It initiates where the electrical field is strongest, and expands through the medium, typically in a bushed, or branched, fashion. An analogy to lightning can be made. Lightning begins with a branched channel of ionized air, which grows from the sky towards the earth. If it reaches the earth, it can act as a conducting bridge, and an electrostatic discharge occurs. Streamers in liquids can qualitatively act the same way. However, the high density of the medium, and the phase transition from liquid to gas, complicates the situation.

1.2 Dielectric breakdown

Two important characteristics of dielectric materials are the dielectric constant, which describes the polarizability, and the dielectric strength, which describes how high electric stress the material can withstand without breaking down. When the dielectric strength is exceeded, the material loses its insulating abilities and begins to conduct electricity rather well. This is known as dielectric breakdown.

The dielectric breakdown may result in an electrostatic discharge, or a continuous electric arc, throughout the medium. However, a partial discharge, i.e. a discharge over a limited section of the medium, can also occur. Partial discharges are often caused by voids in the

material, due to imperfections such as air gaps in solid insulators or bubbles in liquid insulators. The difference in the dielectric constant makes the electric stress higher in these voids and this can cause a local dielectric breakdown, resulting in a discharge across the void. These discharges can cause permanent damage to solid dielectric materials, such as paper and plastic, often through a process called electrical treeing. This process occurs when successive partial discharges over time causes the material to deteriorate close to a void, which in turn causes the void to gradually expand, resulting in a tree-like structure.

Discharges usually destroy solid insulators, either partially or completely. Liquid insulators however, are self-repairing, as its molecules are not in a fixed position. Here, the defect created by a discharge will not stay in place, and mechanisms like treeing cannot occur. The streamer mechanism may resemble treeing, but the timescales are completely different. A streamer is a fast and quasi-continuous event.

1.3 Research methods

Dielectric breakdown in liquids has been subject to research over many decades. Experimental setups typically consist of two electrodes submerged in liquid, a high voltage generator, and various measurement instruments. Different electrode configurations are used, such as plane-plane, sphere-sphere, and needle-plane. These configurations give rise to different types of electric fields. The electric field between two ideal planar electrodes is uniform, while the field from a sphere-sphere or needle-plane configuration is divergent. The needle-plane configuration is also asymmetrical; the electric field is extremely strong and divergent around the needle electrode, compared to the planar electrode.¹⁰ This enables us to investigate the mechanisms of positive and negative polarity individually. Other types of experiments may include geometrical constraints, such as pressboards or tubes.^{7,11}

There are many different ways to apply electrical power to the systems mentioned above, but experiments often fall into three main categories: gradual increments, lightning impulse, and step voltage. In the first method, gradual increments of the voltage, could be either AC or DC, and starts at a low voltage that is increased until a breakdown oc-

curs. A lightning impulse has a voltage–time curve with a fast rise to a high voltage (microsecond scale), and then a slope down to zero voltage. The test is designed to simulate power surges due to lightning. It tells something about another important aspect of electrical breakdown, namely that a breakdown requires time to happen. Equipment can withstand voltages significantly higher than the breakdown voltage, as long as the time is sufficiently short. The third method, step voltages, has a voltage–time curve with rise from zero to the maximum voltage that is as sharp as possible (nanosecond scale), and then preferably maintaining the voltage for the duration of the experiment.

The first two methods are used for benchmarking of electrical equipment and insulating materials. However, step voltage is the preferred method for trying to explain the fundamental mechanisms of a breakdown, since it gives better control of the main variable, the voltage. That said, the actual main parameter is the electric field strength, which is given by both the applied voltage and the geometry.

Experiments and benchmarking are costly, both with regards to money and time. This is where numerical simulations enter the picture: A good numerical model could be used to simulate the behavior of different liquid compositions, and thus indicate which of the compositions that are worth benchmarking.

SINTEF has developed a numerical model for streamer propagation¹² based on the Townsend–Meek criterion. The model is able to simulate several of the properties of a streamer, as well as the effect of additives. Several other models exists as well, from simple models for isolated properties, such as shape or structure,^{13–15} to more rigid and time consuming simulations.^{16,17}

1.4 Motivation

Streamers in liquids are studied in order to better understand the underlying mechanisms. By knowing the roles that the various parameters play, better methods for protection of equipment can be developed, and good candidates for insulation liquids can be identified. This is a far more proactive approach to the problem than to simply benchmark all configurations and insulation liquid candidates.

Results from SINTEF's present model mimics the trends observed in of experiments second mode streamers. The model gives a propagation voltage that is somewhat too high, and a lower degree of branching than expected. It also fails to replicate the transition to the fast propagating fourth mode at high voltages.¹⁸

Implementation of energy calculations and photoionization have been proposed to improve the model. This thesis proposes a model for photoionization and explores how this will affect the model. Effects from photoionization may possibly be able to explain the rapidly growing streamers at high voltages. It might also play a role in the branching process of the streamer. In addition, the basis of the model, the Townsend–Meek criterion, is explored. This is done by comparing the currently used criterion to data available in literature, and by looking at how the criterion affects the model.

In the future, the hope is that the model should be able to predict the most important aspects of streamers in different liquids, with various additives.

1.5 Scope and structure

This chapter contains general background information and the motivation for the work done in this report. In chapter 2, an introduction to the theory of streamers in liquids is presented. The most important results from experiments, and their implications, are outlined. Ionization mechanisms are important in electric breakdown theory. As such, the specific mechanisms that are important for this thesis are presented. The numerical model relevant for this work is outlined in chapter 3. The Townsend–Meek criterion, which the model is built upon, is also described. Then, the possibility of expanding the model by including the effect of photoionization, is explored. The most important results of the formulas derived in chapter 3 are presented in chapter 4. These results are discussed in chapter 5, along with the implications of choosing different methods or parameters. Finally, a conclusion is included in chapter 6, and suggestions for further work are given in ??.

Chapter 2

Background theory

2.1 Streamers in liquids

Streamers in liquids is a field of research that involves multiple disciplines and phenomena occurring on many different scales. We will focus on streamers in a needle-plane gap, with positive polarity on the needle. These conditions are most relevant for the present numerical model. The needle-plane configuration ensures a strong electric field in the vicinity of the needle, which makes it possible to know where the streamer will initiate, and to investigate positive and negative polarities separately. This geometry is further explained in section 3.1. Both positive and negative polarities are interesting to research. The polarity with the lowest breakdown voltage, the positive polarity, is the one given the most attention, because streamer research is primarily

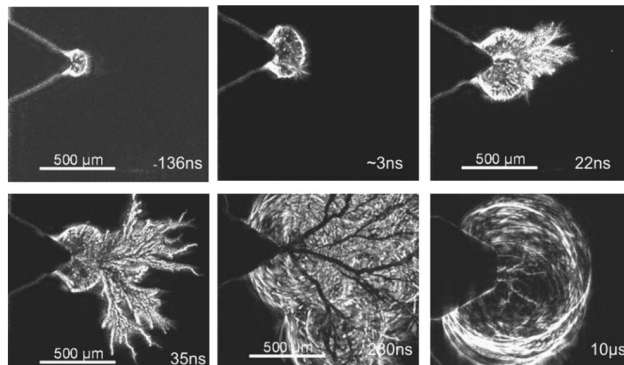


Figure 2.1: Schlieren images of the development of a streamer in water, needle-plane electrode geometry. The images are qualitatively similar to streamers in cyclohexane and transformer oils. Figure 5 from AN, BAUMUNG, AND BLUHM.¹⁹

focused on protecting materials from electrical discharges.

Figure 2.1 depicts the initiation and propagation of a streamer. The first two pictures show the initiation of the streamer; i.e. a small bubble growing at the tip of the needle. The voltage required for this to occur is called the initiation voltage. At voltages above the initiation voltage and below the breakdown voltage, the streamer propagates a certain length into the medium, before stopping. In the next two pictures in fig. 2.1, the streamer is propagating from the bubble in a bush-like fashion, and in the fifth picture a filamentary streamer is seen as dark branches above the illuminated pressure waves.

Increasing the voltage increases the stopping length, and increasing the external pressure reduces it.⁴ The critical voltage that enables a streamer to close the gap, and thus cause a breakdown, is known as the breakdown voltage.

The speed of the streamers is only weakly dependent on the voltage,⁶ as long as the voltage stays below a certain threshold. The voltage where a streamer becomes highly dependent on the voltage is known as the acceleration voltage. The acceleration voltage is typically twice the breakdown voltage for transformer oils, but for natural esters they can be almost equal.⁹ The streamer phenomenon is of stochastic nature, hence the initiation voltage, breakdown voltage, and acceleration voltage are the voltages fitting the given criteria for 50 % of the experimental streamers.

The two final pictures in fig. 2.1 focus on the pressure waves that propagate from the streamer. This is an interesting phenomenon, but not one we will look further into. One of the main streamer phenomenon not seen in fig. 2.1 is that some streamers are luminous. For luminous streamers, the whole channel or just the tip, is either continuously or sporadically luminous.

2.1.1 Propagation modes

LESAIN AND MASSALA⁶ defined four modes of streamer propagation in liquids. These are based on the appearance of the streamer and the order of magnitude of the propagation speed. The first mode is a slow growing bubble or bush with a speed of the order 100 m/s. This mode is typical for very sharp points,³ and will usually not lead to a

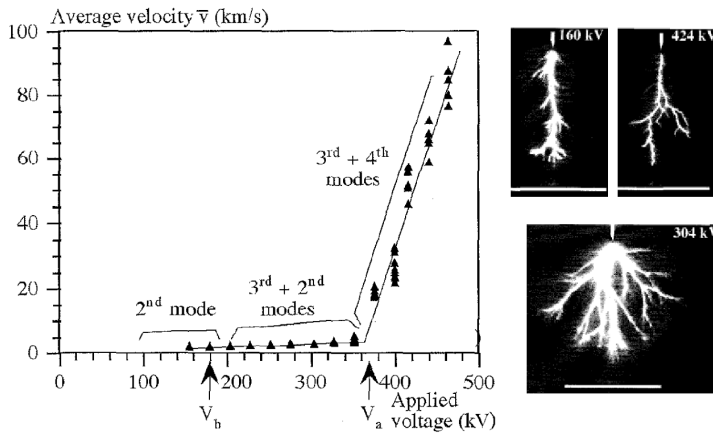


Figure 2.2: Streamer speed and shape as a function of voltage. The top left of the pictures is for 160 kV, the top right for 424 kV, and the bottom one for 304 kV. This is for transformer oil in a gap of $d = 100$ mm. Taken from figs. 4 and 6 in LESAIN AND MASSALA.⁶

breakdown by itself. For low voltages, it can only propagate a small distance into the medium, before the electric field strength becomes too low, and the propagation stops.

For higher voltages, a transition from the first to the second mode can occur, or the streamer can initiate as a second mode. This mode is seen for voltages both below and above the breakdown voltage. The second mode looks more filamentary, or branched, and propagates with a speed of the order 1 km/s. Another characteristic is that the speed has only a weak dependence on the voltage. Increasing the voltage tends to increase the number of filaments, rather than increase the speed (see fig. 2.2). Sporadic or periodic illuminations, associated with a spike in the current, is often seen from this mode.

Voltages above the breakdown voltage can initiate the third mode streamer. This mode has a propagation speed of the order 10 km/s, has numerous branches, and will often experience a higher frequency of illuminations than the second mode. For voltages below the acceleration voltage the third mode typically switches to the second mode at some point. This makes the average speed of the streamer dependent

on how long the streamer propagated as a third mode, and this length increases with increasing voltage.⁶

The third mode switches to the fourth mode for voltages above the acceleration voltage. The transition is associated with a reduction in filaments, from numerous to a few very luminous filaments (see fig. 2.2). However, increasing the voltage increase the number of filaments for this mode as well. The fourth mode has a propagation speed above 100 km/s. The average velocity of a streamer for voltages above the acceleration voltage depends on how far the streamer propagates as the third mode, which in turn depends on the voltage.

2.1.2 Propagation mechanisms

The first mode of propagation is often explained as a process where Joule heating causes the formation of gas cavities.²⁰ Electrons accelerated in the electric field heat the medium through collisions. This causes the nucleation of bubbles, and electric discharges over the bubbles extend the electric potential from the needle tip into the medium.

The higher propagation modes are fast events, and are approached with two different methodologies: it is either argued that the events happen fast enough for the liquid to be approximated as a solid, or that a dense gas approximation can be applied.²¹ In the solid approximation, the liquid is described as a semiconductor, with a valence band, conduction band, and band gap. Electrons assumed to occupy either trapped or quasi-free states. A positive streamer extracts electrons from the medium, and holes are left behind. Electrostatic cracking occurs when the density of holes reaches a critical limit.²² This process lowers the density and enables partial discharges, which move the electrode potential further into the medium. Then the process repeats.

A positive streamer is a sequential process in gas theory as well (see fig. 2.3). The first step of the process is that electrons are accelerated by a strong electric field. These electrons may then ionize molecules in their path on impact, resulting in more and more free electrons, known as an electron avalanche. The avalanche mechanism is explained in more detail in section 2.2.2. Note that the ions have low mobility compared to the electrons, and are left quasi-stationary. These ions create an extension of the streamer's electric potential, and cause new

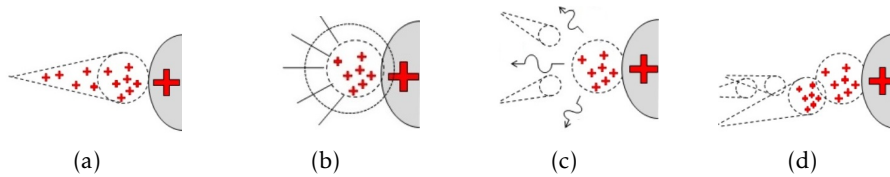


Figure 2.3: Propagation of a streamer in gas. (a) Initial avalanche from seed electron. (b) Field enhancement from ions. (c) Photons emitted and new avalanches started. (d) Sequential avalanches leaving ions behind. Adapted figure from ILDSTAD.²³

electron avalanches. The streamer grows by adding up the charge of sequential electron avalanches.

Electron avalanches in the liquid phase is a controversial topic. In gas the avalanche mechanism is highly dependent on the mean free path, which is very short in liquids. To make up for the shortness of the free path, a very strong electric field is required to get electrons accelerated to energies high enough for impact ionization. This is nevertheless the methodology that the numerical model of `SINTEFIS` based upon.

2.2 Ionization

A neutral atom or molecule is ionized when it loses or gains an electron, turning it into a positive or negative ion, respectively. Ionization can be caused by various processes such as impact ionization, field ionization, photoionization, radioactive decay, or by absorbing an electron. The process can be stated as:



where A is a molecule, e^- is an electron, and A^+ is a positive ion. The energy required to free an atom or molecule's electron from its bound state is called ionization potential (IP). The ionization potential of a molecule can be found by taking the energy difference between the system before and after ionization:

$$I_A = U_{A^+} + U_{e^-} - U_A. \quad (2.2)$$

In this equation, I is the ionization potential, U is the energy, and the subscripts have already been explained above.

Ionization mechanisms play an important role in electrical discharges. For gases, impact ionization is the main contributor to the Townsend discharge mechanism, and photoionization plays an important role for streamer breakdown. The latter is dominant when the electric field is divergent.

The same mechanisms are considered important in liquids as well, and liquids are therefore often treated in the dense gas approximation. Streamers in liquids are sometimes viewed as ionizing waves propelled by field ionization,²⁴ and other times as successive electron avalanches in front of the streamer, in ionizes the medium and builds up charge. In this picture, photoionization is also thought to play a role, especially for fast events (third and fourth mode). However, there is currently no consensus about the exact mechanisms and when they are dominant.

Electronegativity is used to describe the ability of an atom or molecule to absorb an electron and form a negative ion. Substances with high electronegativity, such as sulfur hexafluoride, are preferred as insulators because they can inhibit electron avalanches by absorbing free electrons.

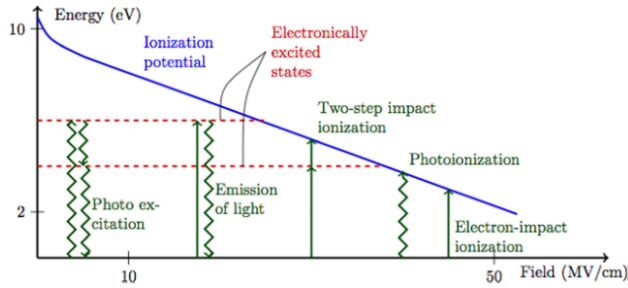


Figure 2.4: This sketch qualitatively depicts how the IP is reduced as a function of the electrical field strength, and highlights several processes important for ionization. Wavy lines denote photons and solid lines denote impact by electrons. The positions of various processes are chosen only to make the sketch clearer, e.g. impact ionization can also occur at zero field. Adapted from fig. 1 from DAVARI ET AL.²⁵

2.2.1 Field ionization

Electrons are bound to their atom or molecule by the Coulomb potential. Neutral molecules are quite stable; the probability of electron emission is very low. However, this probability is increased in the presence of an electric field. The electric field lowers the potential barrier in the direction of the field, making it easier for tunneling to occur. The tunneling time τ follows the electric field strength E as:²⁶

$$\ln \tau \sim \frac{1}{E}. \quad (2.3)$$

That an electric field reduces the potential barrier also implies that the IP is a function of the electric field. This effect has recently been looked into specifically for substances relevant for electrical insulation.^{25–28} The relation can be calculated exactly for a hydrogen atom:

$$I(E) = I_0 - \beta \sqrt{\frac{E}{\epsilon_r E_{a_0}}}. \quad (2.4)$$

Here, I_0 is the zero field IP, β is a parameter depending on the molecule, ϵ_r is the relative permittivity, and $E_{a_0} = 5.14 \times 10^{11}$ V/m. This relation

can to a good approximation also be used to model the field dependent IP of more complex molecules. Curve fitting of (2.4) to match data from DAVARI ET AL.²⁸ gives $\beta = 50.8$ eV with a RMSD of 0.2 eV for cyclohexane.^a In comparison, $\beta = 54.4$ eV for the hydrogen atom.

Although the electric field has an effect on the IP it does not seem to have any big effect on the energy of excited states below the IP energy.²⁸ Figure 2.4 indicates how the IP is reduced by the electric field while the electronically excited states stay constant. Depending on strength, an electric field will remove the possibility of one or more excited states, and ionize any molecule excited to a state above the field dependent ionization potential.

2.2.2 Impact ionization

Impact ionization happens as a result of a collision where the kinetic energy provides the ionization energy. A general collision between two objects, of mass m and velocity v , is described by:

$$\frac{1}{2}m_1v_1^2 + \frac{1}{2}m_2v_2^2 = \frac{1}{2}m'_1v_1'^2 + \frac{1}{2}m'_2v_2'^2 + \Delta U. \quad (2.5)$$

If the energy difference ΔU equals zero, then the collision is said to be elastic. An inelastic collision results in a positive energy difference. The systems we normally consider consist of heavy molecules and some few free electrons in a strong electric field. The electron mass is far less than the mass of the molecules, this makes them far more mobile than the molecules. As such, the molecules can be considered stationary while the electrons rapidly gain speed.

An electron striking a molecule is the only type of collision important enough to consider. Elastic collisions between these particles generally result in both keeping their initial energy; the electron scatters off the molecule, while the molecule stays in place. However, an inelastic collision implies that the electron loses some of its kinetic energy. This energy could excite molecular vibrations, excite electrons in the molecule, or ionize the molecule.

^aThe calculations was based on data N. Davari kindly provided through private channels.

In the presence of a strong electric field, it is possible for the average electron to ionize one or more molecules before being absorbed. The result is an avalanche effect where one initial seed electron is multiplied into numerous electrons. The differential equation for such a system reads:

$$dN_e = \alpha N_e d\ell. \quad (2.6)$$

Here, N_e is the number of electrons in the avalanche, ℓ is the distance, and α is the first Townsend coefficient, which represents the net ionization per unit length. This coefficient is generally dependent on the electron's free mean path and the electrical field strength, $\alpha = \alpha(E, \lambda_{\text{FREE}})$. The free mean path is dependent on both the collisional cross section and density of the substance. The latter implies that α is dependent on the pressure in gases, however, in a liquid it only depends on the electrical field. For liquids it is assumed that:²⁹

$$\alpha = \alpha_{\text{MAX}} \exp\left(-\frac{E_\alpha}{E}\right), \quad (2.7)$$

where α_{MAX} and E_α are liquid dependent parameters that are found experimentally.⁸ For liquid cyclohexane, data from HAIDARA AND DENAT³⁰ give $\alpha_{\text{MAX}} = 2 \times 10^8 \text{ m}^{-1}$ and $E_\alpha = 30 \times 10^8 \text{ V/m}$.

Equation (2.6) is fairly easy to solve for systems with a uniform electric field, $N_e = N_0 \exp(\alpha \ell)$, where N_0 is the initial number of electrons and ℓ is the length of the avalanche. For the more general case we have to use the full equation:

$$N_e(\ell) = N_0 \exp\left\{\int_0^\ell \alpha d\ell'\right\}, \quad (2.8)$$

which in general cannot be solved analytically. The length of the avalanche could be taken as the gap distance between two electrodes, or the region where the field is high enough for electron multiplication to occur. The former is typically used for Townsend discharge, while the latter is more relevant for streamer discharge where the electric field is divergent. Equation (2.8) is related to the Townsend–Meek criterion, which will be explained in section 3.3.

2.2.3 Photoionization

Photoionization is responsible for the photoelectric effect. A photon γ with high energy is absorbed by an atom or a molecule A , and an electron e^- is emitted:



When photons with energy below the IP are absorbed, a vibrational state can be excited or an electron can be excited to a higher orbital. On the other hand, an atom or molecule relaxing from an excited state emits a photon. These effects are illustrated with curvy lines in fig. 2.4. A bound–bound transition is only allowed if the momentum is conserved, and the transition probability is highest when the energy difference between the states is the same as the photon energy. Photoionization implies a transition from a bound to a free state for the electron. The free state is a continuum, represented by the momentum of the electron. This is generally the case for bound–free transitions as well, however, instead of just a sharp peak, the probability rises rapidly as the photon energy approaches the ionization energy and then drops slowly when the energy is increased further. Here, slowly is implied only as a comparison to the sharp rise.

The transition probability is related to the cross section σ , which is more convenient to use in our case. Conventionally, one finds the differential cross section $d\sigma/d\Omega$, which is the probability of emitting an electron per solid angle, and integrate it over all angles to find the total cross section. Here however, we will do this a bit differently. We assume that the cross section is separable:

$$\sigma = \sigma_0 \sigma_\omega \sigma_\Omega , \quad (2.10)$$

were, σ_0 is the cross section at the IP, σ_ω is dependent on the photon frequency, and σ_Ω is angle dependent. By writing the expression this way, the two latter factors are normalized. Experimental values for σ_0 in noble gases are typically in the order of megabarns³¹ (1 Mb = 10^{-22} m²).

The frequency dependent cross section for a simple hydrogen atom can be calculated to:^b

$$\sigma_{\omega} \sim \begin{cases} 0 & \text{for } \hbar\omega < I, \\ \omega^{-3} & \text{for } \hbar\omega \geq I. \end{cases} \quad (2.11)$$

Here, $\hbar\omega$ is the photon energy, and I is the ionization potential.

The differential cross section $d\sigma_{\Omega}/d\Omega$ is dependent on the angle θ between the photon momentum vector and the emitted electron's momentum vector, and follows the relation:^c

$$\frac{d\sigma_{\Omega}}{d\Omega} \sim \sin^2 \theta. \quad (2.12)$$

This equation states that the electron emission probability is highest in the directions perpendicular to the momentum of the photon, i.e. in the direction of the photon's electric field. The equation is not valid in the presence of an electric field. In section 3.4.1 however, it is modified in an attempt to include the effect of an external electric field.

^bFor the full equation see B. RYBICKI AND P. LIGHTMAN³² page 284.

^cFor the full equation see MERZBACHER³³ page 502.

Chapter 3

Numerical model

In this chapter we first define the geometry that is used for the model, and give some of its main properties. Then, the general concepts of the present model is explained, and its main idea, the Townsend–Meek criterion, is explored further. A method to implement photoionization in the model is presented in the final part.

3.1 Geometry

The model mimics a needle–plane configuration, i.e. a needle electrode above a planar grounded electrode (see fig. 3.1). The configuration causes a strong, divergent electric field in the vicinity of the needle

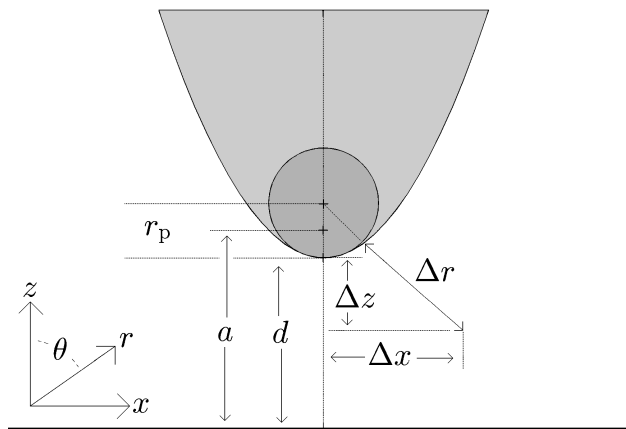


Figure 3.1: Variables in the needle–plane geometry. The distance between the needle and the plane is usually far greater than the impression given by this figure.

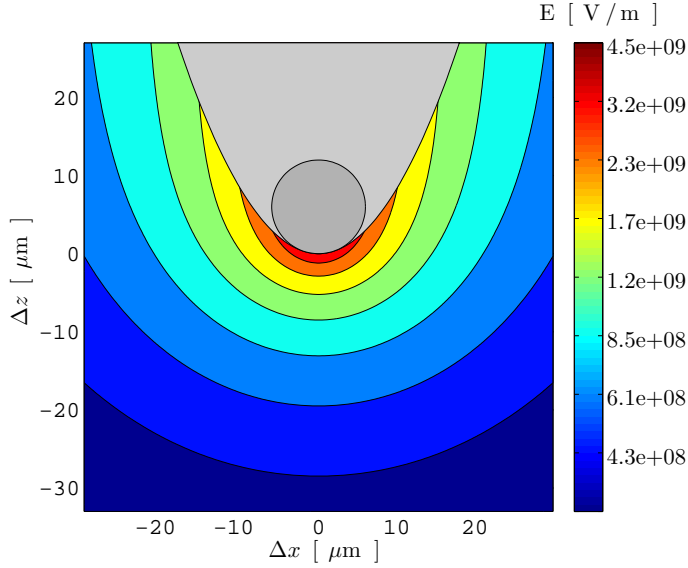


Figure 3.2: Electric field around a hyperbolic needle, for $d = 10\text{mm}$, $r_p = 6.0\mu\text{m}$, and $V_0 = 120\text{kV}$. The circle in a darker shade of gray has $r = r_p$.

tip (see fig. 3.2.) A rotationally symmetric hyperbolic needle is used. This configuration makes it possible to solve the Laplacian equation for the electric field analytically in prolate spheroid coordinates. Prolate spheroid coordinates are explained in appendix A, and more details are found in COELHO AND DEBEAU.¹⁰

Figure 3.1 shows the setup of a hyperbolic needle with tip curvature r_p , separated from a plane by a distance d . The origin of Cartesian coordinates is taken to be where the central axis of the hyperbola intersects with the plane. This implies that the tip of the needle is located at $z = d$, the focal point of the hyperbola is located at $z = a$, and the center of the sphere, which is tangential to the curvature at the needle tip, is located at $z = d + r_p$, while $x = y = 0$ for all these points. The notation $\Delta x, \Delta y$, and Δz is used to refer to distances relative to the tip of the needle. With the chosen origin, $\Delta x = x$, $\Delta y = y$, and $\Delta z = z - d$.

The variable r is used in two different ways. The first use is in formulas approximating the electrical field along the central line of

the hyperbola, i.e. $x = y = 0$ and $\theta = \pi$. Here, r is the distance from $(x, y, z) = (0, 0, a)$,

$$r = a - z. \quad (3.1)$$

In this notation is $r_0 = r_p/2$ at the tip of the needle.

The second use of r is for the distance from the center of the circle at $(x, y, z) = (0, 0, d + r_p)$,

$$r = \sqrt{x^2 + y^2 + (z - d - r_p)^2}. \quad (3.2)$$

This origin is used when modeling photoionization. In this notation, the surface of the needle is located at $r = r_0$, and r_0 is a function of θ . For the central axis, i.e. $\theta = \pi$, $r_0 = r_p$. The notation Δr is also used for photoionization. It describes how far into the fluid a photon has traveled, $\Delta r = r - r_0$. The angle θ is always defined by $\cos \theta = \hat{z} \cdot \hat{r}$.

3.2 The present numerical model

SINTEF has developed a script for simulating positive streamers in a needle–plane geometry. The model is described in HESTAD ET AL.¹² and is based upon the work done by INGEBRIGTSEN ET AL.⁸

The model is currently based on cyclohexane as the insulating liquid. Cyclohexane has somewhat similar properties to commonly employed transformer oils, but it is well-described and a much simpler chemical composition. This reduces the number of independent parameters, and makes it easier to compare the results from the model with experimental results.

The script is focused on the processes occurring in front of the streamer tip, and not the dynamics of the channel or the plasma–liquid interface. The tip of the streamer is modeled as a hyperbolic needle. This will often be referred to as the “streamer head”, and the “forward direction” or “in front” means towards the plane electrode, i.e. $\theta = \pi$.

The streamer head is initially the needle, but during propagation of the streamer a hyperbolic needle of $r_p = 6.0 \mu\text{m}$ is used as the streamer head. This tip radius is considered to be the critical size for inception of second mode streamers.³ The first mode is not seen for tips above this size, either the second mode or a higher mode is initiated directly. One interpretation is that tip of the second mode streamer can be modeled as a tip of this size.¹²

The simulation begins with a random distribution of negative seed ions, see fig. 3.3. The density of seed ions is based on the low field conductivity of the liquid, and this initial random distribution gives rise to the stochastic property of streamers. The main part of the simulation is a while-loop, which continues until a streamer head reaches the grounded electrode.

All of the seeds are moved in the electric field according to their mobility. A seed is considered to be an ion when the electric field strength is low, and to be an electron when the field strength is above a given threshold. The seed electrons are multiplied as a function of the local electric field strength and the distance traveled. If a seed electron that has multiplied to an electron avalanche above a certain value is considered as a part of the streamer. The streamer head is then moved to the position of the avalanche. The threshold for when an avalanche

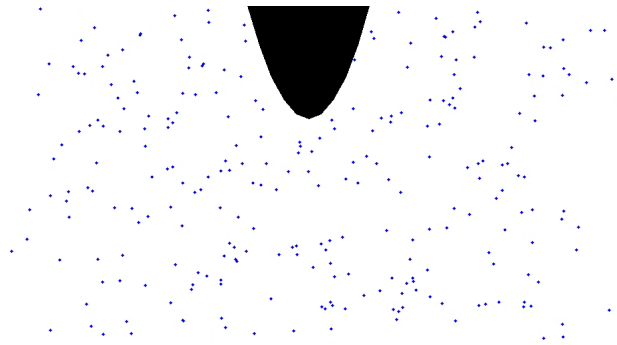


Figure 3.3: This is one realization of the distribution of seed ions used by the model. The 3D distribution is here projected on to a 2D surface.

is considered a part of the streamer is given by the Townsend–Meek criterion.

If a seed behind the streamer head reaches the threshold then that seed is considered as a new streamer head. This is the criterion responsible for branching in the model. However, a new head can only originate at given a minimum distance from the current head. The same criterion is used to combine two streamer heads if they get too close.

The electric field from a streamer head is calculated in two steps. First the potential of each propagating head is set to a lower value than the needle by assuming that the potential has a constant gradient along the streamer channel. Secondly, the electric fields from all the heads are integrated from each of the heads and to the planar electrode. Then the potential of each streamer head is scaled by the ratio between these two potential. This accounts for the shielding effect between the different heads.

The main results from this model include the shape of the streamers, average and instantaneous speed, inception delay and breakdown probability. In order to improve the quality of these results it has been proposed to investigate the dynamics of the streamer channel, and to include energy and photoionization considerations.

3.3 The Townsend–Meek criterion

Equation (2.8) gives the number of electrons in an avalanche, and this tells something about the nature of the discharge. In gases, Townsend and streamer discharge mechanisms typically involve electrons in the order of 10^4 and 10^8 , respectively.³⁴ In most cases we assume that the avalanche originates from a single electron, referred to as a seed electron. Possible sources of this electron include ionization by cosmic radiation and ions releasing an electron upon entering an area of high electric field strength.

For an avalanche starting from a single electron, all the information needed is in the exponent of (2.8). The equation,

$$Q_c = \int_0^\ell \alpha \, d\ell', \quad (3.3)$$

is known as the Townsend–Meek criterion. Here, Q_c is the Meek constant, α is the first Townsend coefficient, and ℓ is the length of the avalanche. Using the values mentioned above, $Q_c = \ln(10^8) \approx 18$ for a streamer breakdown in gases. For liquid cyclohexane however, INGEBRIGTSEN ET AL.⁸ found $Q_c = 23$ by considering a gap of $d = 10$ mm, a hyperbolic needle of tip radius $r_p = 6 \mu\text{m}$, and $V_0 = 33$ kV for the propagation voltage of second mode streamers. The critical tip radius for inception of second mode streamers was based on GOURNAY AND LE-SAINTE.³ However, the propagation voltage is not well-defined; various values have been reported.^{3,35} The variations are probably a result of differences between experimental setups, and the interpretation of the results.

There is no general analytical solution to (3.3), but some approximations can be made. Along the central line, $\theta = \pi$, and close to the needle tip, $r \ll d$, the electrical field can be approximated to:

$$E(r) = E_0 \frac{r_0}{r}. \quad (3.4)$$

Here, E_0 is the electric field strength at the needle tip, where $r = r_0$. More details can be found in appendix A.2. In combination with the equation $\alpha = \alpha_{\text{MAX}} \exp(-E_\alpha/E)$ from (2.7) we find the maximum size

possible for an avalanche Q_{MAX} to be:

$$Q_{\text{MAX}} = \int_{r_0}^{r_c} \alpha \, dr = \frac{E_0 r_0}{E_\alpha} (\alpha_0 - \alpha_c). \quad (3.5)$$

Here, the subscript c denotes the threshold where the field is strong enough for electron multiplication to occur. However, $\alpha_c \ll \alpha_0$, and α_c can thus often be ignored, which is the same as moving the upper bound of the integral to infinity.

The exact formula for α in the Laplacian field is:

$$\alpha = \alpha_{\text{MAX}} \exp\left\{-E_\alpha \frac{a^2 - z^2}{aC}\right\}, \quad (3.6)$$

where $C = 2V_0/\ln(4d/r_p)$, z is the position, and a , r_p and d are gap parameters. The details for the electric field are included in appendix A.2. Analytical integration of this formula results in a very small prefactor combined with a very large term from the imaginary error function, which is not convenient. Instead, (3.6) will be used when solving (3.3) numerically, in order to validate the approximation (3.5).

In the model, Q_c is used to determine when an electron avalanche is large enough to be considered as a part of the streamer. This is how the streamer grows; by adding together successive avalanches. It is of interest to know which seed electrons that can reach this number, and where they can reach it. With this in mind we define two new variables:

$$Q_i = \int_{r_0}^r \alpha \, dl = \frac{E_0 r_0}{E_\alpha} (\alpha_0 - \alpha_r), \quad (3.7)$$

$$Q_f = \int_r^a \alpha \, dl = \frac{E_0 r_0}{E_\alpha} \alpha_r. \quad (3.8)$$

Here, Q_i describes the maximum value an avalanche initiating from a position can achieve, and Q_f describes the maximum value of an avalanche at a position. The two regions $Q_i \geq Q_c$ and $Q_f \geq Q_c$ is where an avalanche can originate in order to reach critical size, and where it is possible for an avalanche to reach the critical size, respectively.

The equations (3.7) and (3.8) are valid approximations along the central, but it is possible to make the definition of Q_i and Q_f more general. Prolate spheroid coordinates (μ, ν, ϕ) is used for this purpose, see appendix A for more details. Equation (2.7) is still used for α , but is now used in combination with the exact Laplacian expression for the electric field (A.15),

$$E(\mu, \nu) = \frac{C}{a \sin \nu (\cosh^2 \mu - \cos^2 \nu)^{1/2}}, \quad (3.9)$$

while assuming that an avalanche follows the electrical field lines. This implies that μ is constant, and might be a rough approximation. With this assumption we can use (A.12),

$$d\ell(\mu, \nu) = a \left(\sinh^2 \mu \cos^2 \nu + \cosh^2 \mu \sin^2 \nu \right)^{1/2} d\nu, \quad (3.10)$$

to replace $d\ell$ in (3.3). Putting everything together gives more general formulas for the two variables:

$$Q_i = \int_{\nu_0}^{\nu} \alpha [E(\mu, \nu)] d\ell(\mu, \nu), \quad (3.11)$$

$$Q_f = \int_{\nu}^{\pi/2} \alpha [E(\mu, \nu)] d\ell(\mu, \nu). \quad (3.12)$$

These equations are easily solved numerically and should provide some information on where the interesting seed electrons are, and where avalanches can be considered as a part of the streamer, as a function of the geometry and the applied voltage.

3.4 Photoionization model

The third and fourth modes are often very luminous. Photoionization is thought to play a part in the transition to, and the propagation, of these modes.^{7,36} The high speed could be obtained through high ionization rates close to the streamer, efficiently expanding the streamer. This is most relevant if the photoionization is very localized, i.e. the radiation is absorbed within a short distance. However, the high speed could also be obtained through a feed-back mechanism, where photoionization provides new seed electrons. Increasing the number of available seed electrons increases the propagation speed of the model. The seed electrons generated on the side of the streamer play a part in branching process of streamers.

In the first part, we make some assumptions on how the cross section σ is dependent on both the electric field strength and the orientation of the field in relation to a photon. The cross section is required both for the attenuation of the radiation and for calculating the ionization rate. Then, possible sources of radiation are identified; the thermal background radiation, and radiation from molecules relaxing from excited states. These two are our initial sources at the streamer head, they are attenuated as the radiation propagates throughout the medium, and in combination with the cross section, they give the rate of ionization. Finally, the values of the main parameters of the photoionization are given.

3.4.1 Photoionization in an electric field

The equations for σ_ω and σ_Ω , (2.11) and (2.12) respectively, are calculated using quantum mechanical considerations for a hydrogen like atom without the presence of an external electric field. Without an external field, the Schrödinger equation is separable in spherical coordinates and the form of the final state wave function of the free electron is equal in all directions. Also, an electron can never truly escape the Coulomb potential. Adding an external electric field changes the situation. In a constant electric field of uniform strength, the Schrödinger equation is separable in parabolic coordinates,³⁷ and the final state wave function of the free electron is angle dependent. This type of

formalism is not pursued any further in this work, instead, we will try to make approximations based on what we know from sections 2.2.2 and 2.2.3.

We start by setting up our system, see fig. 3.4, oriented to have the electric field pointing in the z -direction, $\mathbf{E} = E\hat{z}$. Equation (2.4) describes how the IP is reduced in the direction of the field, but for an arbitrary direction we need to modify the equation to accompany the angle θ_e between the electric field and the emitted electron:

$$I(E, \theta_e) = I_0 - \beta \sqrt{\frac{E}{\epsilon_r E_{a_0}}} \cos \theta_e. \quad (3.13)$$

Consequently, for a given electric field strength E and photon energy $\hbar\omega$, we find the classical allowed area, defined by $I(E, \theta_e) < \hbar\omega$. The upper bound of θ_e is then given by Θ , according to:

$$\cos \Theta = \frac{I_0 - \hbar\omega}{\beta} \sqrt{\frac{\epsilon_r E_{a_0}}{E}}. \quad (3.14)$$

A value of $\Theta \in [0, \pi/2]$ implies that the photon energy is below the initial IP. Without an external field the allowed area for these energies is zero, but the allowed area increases as the electric field strength exceeds above a certain threshold. In contrast, a value of $\Theta \in [\pi/2, \pi]$ implies that the photon energy is above the initial IP, and here, an increase in the electric field reduces the allowed area. The effect is an increase in absorption for frequencies below the IP, and a decrease for those above the IP, as a function of electric field strength. The effect on the high energy photons is not desirable and the area is quantum mechanically forbidden. As such, this region is excluded and only the first area, $\Theta \in [0, \pi/2]$, is considered.

In zero field, the electron emission probability is highest in the direction of the photon's electric field, i.e. perpendicular to the photon's momentum k_γ . The relation is given by (2.12). In our reference system, fig. 3.4, the angle between the absorbed photon and the emitted electron is given by $\hat{k}_\gamma \cdot \hat{k}_e = \cos(\theta_\gamma - \theta_e)$. We find the angular dependence of the cross section in an electric field by integrating the angular differential cross section (2.12) over the allowed angles:

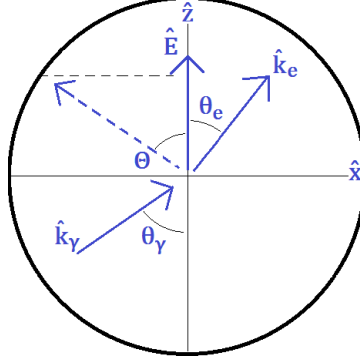


Figure 3.4: Photoionization coordinate system.

$$\sigma_{\Omega} = C_{\Omega} \int_0^{2\pi} \int_0^{\Theta} \sin^2(\theta_{\gamma} - \theta_e) \sin \theta_e d\theta_e d\phi. \quad (3.15)$$

Here, C_{Ω} is a normalization constant, which is found by demanding $\sigma_{\Omega} = 1$ for $\cos \Theta = 0$ and $\theta_{\gamma} = 0$. Solving the integral yields:

$$\sigma_{\Omega} = 1 - \frac{1}{4} (1 + \cos^2 \theta_{\gamma}) (3 \cos \Theta - \cos^3 \Theta) - \frac{1}{2} \sin^2 \theta_{\gamma} \cos^3 \Theta. \quad (3.16)$$

The details of the calculation are shown in appendix B. This expression for σ_{Ω} equals zero for photon energies below the field reduced IP, where $\cos \Theta = 1$, and equals unity for energies above the zero field IP, where $\cos \Theta = 0$. A transition dependent on θ_{γ} occurs in between these two points.

In order to keep the definition $\sigma = \sigma_0 \sigma_{\omega} \sigma_{\Omega}$ from (2.10), σ_{ω} from (2.11) is redefined to:

$$\sigma_{\omega} = \begin{cases} 1 & \text{for } \hbar\omega < I_0, \\ \left(\frac{I_0}{\hbar\omega}\right)^3 & \text{for } \hbar\omega \geq I_0. \end{cases} \quad (3.17)$$

With this definition, σ_{ω} is scaled to 1 at $\hbar\omega = I_0$, and σ 's cut-off for energies below the IP is replaced with a transition given by σ_{Ω} .

3.4.2 Radiation

We need to identify sources of radiation, and possibly their magnitudes. The streamer itself is considered a channel of partly ionized plasma,⁴ with a temperature exceeding that of the surrounding medium.³⁸ As such, we will assume a spectral radiance B_p from the streamer according to Planck's law for a black body:

$$B_p = \frac{2hc^2}{\lambda^5} \frac{1}{\exp\left(\frac{hc}{\lambda k_B T}\right) - 1}. \quad (3.18)$$

Here, λ is the photon wavelength, h is the Planck constant, c is the speed of light, k_B is the Boltzmann constant, and T is the absolute temperature.

Note the difference between spectral radiance and intensity, as these are often carelessly interchanged. Spectral radiance B is power per area per wavelength [$\text{Wm}^{-2}\text{m}^{-1}$], or power per area per frequency [$\text{Wm}^{-2}\text{Hz}^{-1}$], and we have the relation $B(\lambda)d\lambda = B(\omega)d\omega$. In this work we use $B = B(\lambda)$, unless explicitly stated otherwise.

Another possible source of radiation is relaxation of excited molecules. A molecule A in an initial state i , relaxing to a final state f , emits a photon γ_{if} with energy $\hbar\omega_{if}$ equal to the energy difference between the two states:



The problem is that the number of excited molecules is not known.

In an electron avalanche, it might be fair to assume that the energy distribution of the electrons is exponentially for high energies. INGEBRIGTSEN ET AL.⁸ used this principle to calculate the effect an additive has on the first Townsend coefficient α . This a rough estimate, as it assumes that the energy lost to excitation and ionization of molecules does not affect the distribution. Nevertheless, we will use the same formulation to approximate the amount of molecules excited by an avalanche.

The amount of excited molecules N_ϵ generated per second, is related to the amount of ionized molecules N_I generated per second:

$$\frac{dN_\epsilon}{dt} \sim \frac{dN_I}{dt} \exp(k \Delta U). \quad (3.20)$$

Here, ΔU is the energy difference between the excited state and the ionization potential, and k is a parameter depending on the liquid. This is essentially a Boltzmann distribution.

The amount of ionized molecules N_I per second equals the amount of electrons N_e generated per second:

$$\frac{dN_I}{dt} = \frac{dN_e}{dt}. \quad (3.21)$$

The number of electrons generated is given by the First Townsend coefficient α , according to (2.7), and the average speed v of the electrons in the avalanche, i.e. the speed of the avalanche. In the model the speed of an avalanche is given by the electron mobility μ_e and the electric field strength E :

$$v = \mu_e E. \quad (3.22)$$

By combining the equations for v and α , the ionization rate is found to be:

$$\frac{dN_e}{dt} = N_e \mu_e E \alpha. \quad (3.23)$$

This in turn gives an excitation rate of:

$$\frac{dN_\epsilon}{dt} \sim N_e \mu_e E \alpha \exp(k \Delta U). \quad (3.24)$$

This could be a good approximation to calculating the excitation rates. However, to calculate the spectral radiance from the avalanches, the lifetimes of the excited states have to be known. Most states excited by photons have short lifetimes. But electrons may excite states that are not allowed by quantum mechanics to relax by emitting a photon. The lifetimes of such states may be long.

Within the streamer itself it has been estimated that 0.1 – 1 % of the molecules are ionized,³⁸ and similar with the avalanches, the number of excited molecules is expected to be far greater. Radiation from these molecules could play a major role in a photoionization process.

For simplicity, we will only consider the first excited state, and thus ignore radiation from states between this energy and the ionization energy. This because the number of molecules excited to this state is far greater than the other states. We will model this by assuming a radiation peak centered at the first excitation energy:

$$B_g = B_{g0} \exp \left\{ - \frac{(\lambda - \lambda_1)^2}{2(\Delta\lambda)^2} \right\}. \quad (3.25)$$

Here, $hc/\lambda_1 = \varepsilon_1$ is the energy of the first excited electron state, $\Delta\lambda$ is the standard deviation of the peak, and B_{g0} is the magnitude of the peak. This model could easily be expanded by adding similar terms from other excitation levels.

The initial spectral radiance B_0 from the streamer is the sum of the radiation due to temperature and the radiation from relaxation of molecular states:

$$B_0 = B_p + B_g, \quad (3.26)$$

and the power per area, p , of the spectral radiance is calculated by integration of B :

$$p_p = \int B_p d\lambda = \frac{2\pi^4 k_B^4}{15c^2 h^3} T^4, \quad (3.27)$$

$$p_g = \int B_g d\lambda = \sqrt{2\pi} \Delta\lambda B_{g0}. \quad (3.28)$$

An intensity is attenuated according to the Beer–Lambert law:

$$\nabla B = -B\sigma\rho, \quad (3.29)$$

where σ is the cross section, and ρ is the density of the medium. The equation can be solved analytically if the intensity is radial, $B = B(r)$, there is no scattering (only absorption), and the density and the cross

section both are constant. The problem is simplified by only considering the radial component of the spectral radiance, and by assuming constant density. The cross section was defined in the previous section, and is dependent on both the photon momentum and the electric field. In addition, all scattering is ignored. Solving the differential equation for B for spherical symmetry yields:

$$B = B_0 \left(\frac{r_0}{r} \right)^2 \exp \left(-\rho \sigma_0 \int_{r_0}^r \sigma_\omega \sigma_\Omega dl \right). \quad (3.30)$$

The spectral radiance B is now a function of wavelength and position, with $B(r = r_0) = B_0$. The expression can be calculated numerically.

As a simplification we will only consider radiation from within the streamer. The radiation is assumed to originate at $z = d + r_p$, and radiate radially outwards. It is important to note that $z = a = d + r_p/2$ is the focus of the hyperbola, while the center of the above defined coordinate system is the center of a sphere with $r = r_p$, placed so that its surface is tangent to the hyperbola at $z = d$. This sphere is indicated as a circle in fig. 3.1, and is also included in most other plots of the needle.

For the numerical model, $\sigma_0 = 0$ within the needle. This way, there is no attenuation between $r = 0$ and the needle surface $r = r_0(\theta)$. However, B still drops off with the square of the distance. Thus, the radiation at the needle surface will be slightly greater at $\theta = \pi$, than at $\theta = \pi/2$. This is of course because the sphere and the needle coincides, $r_0 = r_p$, at $\theta = \pi$, but are apart, $r_0 > r_p$, at $\theta = \pi/2$.

3.4.3 Ionization rate

The ionization rate per volume W is found according to the equation:

$$W = \int \rho \sigma c n_\gamma d\lambda, \quad (3.31)$$

where n_γ is the photon density, and the other variables was defined in the last section. We define the ionization rate per atom,

$$w = W/\rho, \quad (3.32)$$

and use that

$$n_\gamma = \frac{4\pi\lambda}{hc} B, \quad (3.33)$$

to arrive at:

$$w = \frac{4\pi}{hc} \int B\sigma\lambda d\lambda. \quad (3.34)$$

The ionization rate is expected to be highest directly in front of the needle, as this is the area where the spectral radiance is highest. The rate is however, also dependent on the cross section, which is dependent on the electric field direction and magnitude. The electric field and the radiation have the same direction close to the needle. But, for directions other than $\theta = \pi$, their directions differ, especially when moving further away from the needle. The result of this could be a higher ionization rate on the sides than at the front under special circumstances.

3.4.4 Movement rate

The method presented here for finding the movement rate of a streamer, is very simple. All volume effects are ignored, and the degree of ionization p is the only requirement for propagation. The time Δt required to reach this degree of ionization is:

$$\Delta t = \frac{p}{w}. \quad (3.35)$$

This assumes that the ionization process is stationary compared with the speed of the streamer. This formula is used to define the movement rate v_s of the streamer as:

$$v_s = \frac{\Delta r}{\Delta t} = \frac{\Delta r w}{p}, \quad (3.36)$$

where Δr is the distance from the needle into the medium.

3.4.5 Model parameters

In order to get reasonable results we need to define reasonable parameters for our model. A summary of the chosen parameters is given in table 3.1. The gap $d = 10$ mm is of medium size, and the hyperbolic needle of radius $r_p = 6.0 \mu\text{m}$ is set to the critical radius for inception of second mode streamers.³

We have chosen to look at a theoretical liquid, similar to cyclohexane, as the insulator. The temperature in a streamer is assumed to be in order of 10^3 K.³⁹ The chosen value $T = 7.0$ kK is based on light emitted from chlorinated alkane liquids,³⁸ since the actual value is not known.

A first excitation energy of 7.1 eV, and an IP of 10.1 eV, have been calculated for cyclohexane.²⁸ This is the gas phase IP, and the IP of any molecule in liquid cyclohexane is reduced by about 1 eV.²⁷ Because of this, a first excitation energy of 6.0 eV, and an IP of 9.0 eV, have been used in the model. Other excitation levels have been excluded. For the given gap parameters, the voltage $V_0 = 120$ kV results in an electric field strength of $E_0 = 45 \times 10^8$ V/m at the electrode tip, which

Table 3.1: Model parameters

Variable	Magnitude	Description
d	10 mm	Gap distance
r_p	$6.0 \mu\text{m}$	Needle radius
I_0	9.0 eV	Ionization potential
ε_1	5.6 eV	First excitation energy
β	50.8 eV	IP reduction parameter
ρ	0.1 \AA^{-3}	Density
σ_0	10^{-21} m^2	Absorption cross section
V_0	120 kV	Applied voltage
T	7.0 kK	Streamer temperature
B_{g0}	$8 \times 10^{19} \text{ Wm}^{-3}$	First excitation peak magnitude
$\Delta\lambda$	4.0 nm	Standard deviation

theoretically reduces the IP to 5.6 eV.

The zero field cross section for cyclohexane is quite different from the simple model described above.⁴⁰⁻⁴³ According to COOL ET AL.,⁴² the cross section increases gradually from $\sigma_0 = 0$ at 9.9 eV to about $50 \times 10^{-22} \text{ m}^2$ at 11.2 eV. The set value of σ_0 equal to 10^{-21} m^2 is within this range, and implications of reducing or increasing this value will be checked.

We are left with the two most important factors; the height B_{g0} and the width $\Delta\lambda$ of the radiation peak, neither is known. A narrow peak will give a narrow transition in ionization rates, when going from a weak to a strong field, while a wide peak will increase the length of this transition. The value $\Delta\lambda = 4 \text{ nm}$ corresponds to about 0.1 eV, and is arbitrarily chosen to get a sharp peak. The width $\Delta\lambda$ and the peak height B_{g0} give the power of the radiation peak according to (3.28). For the chosen $\Delta\lambda$, the magnitude $B_{g0} = 8 \times 10^{19} \text{ Wm}^{-3}$ corresponds to about 363 W of radiated power for a sphere of $r = 6.0 \mu\text{m}$. In contrast, GOURNAY AND LESAIN⁵ reported a power of 10 W for second mode streamers in pentane. However, our model is supposed to simulate the propagation of higher streamer modes, and a higher power is anticipated for those.

Chapter 4

Results

4.1 The Townsend–Meek criterion

The Townsend–Meek criterion is one of the key features of our model, the value used for Q_c is therefore very important. The formulas presented in section 3.3 are in this section plotted for data available from earlier experiments,^{3,35} and for general conditions relevant for the model. *(The remainder of this page has been left blank intentionally.)*

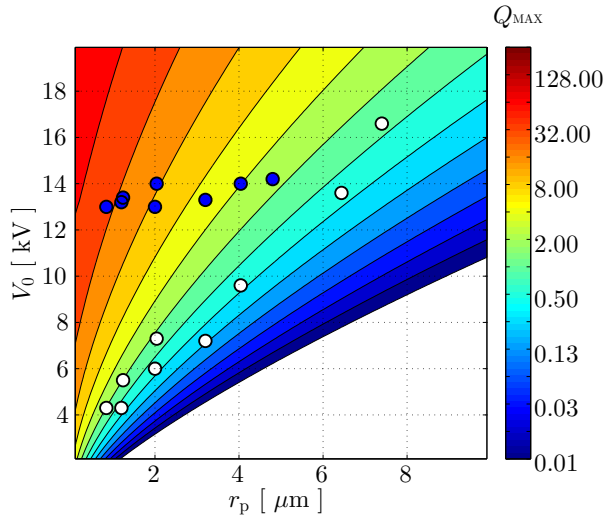
4.1.1 Finding the Meek constant

By using the same input as INGEBRIGTSEN ET AL.,⁸ the approximation (3.5) gives a value of $Q_{\text{MAX}} = 22.6$, and numerical integration of the exact expression (3.6) gives $Q_{\text{MAX}} = 22.7$. Limiting the bounds of the numerical integration, to the tip $r = r_0$ and $\Delta r = r_p/2 = 3 \mu\text{m}$ into the gap, gives $Q_i = 20.6$, which indicates that most of the electron multiplication occurs really close to the tip. These numbers are well in line with $Q_c = 23$, which was found in the article,⁸ and proves that the approximation works well.

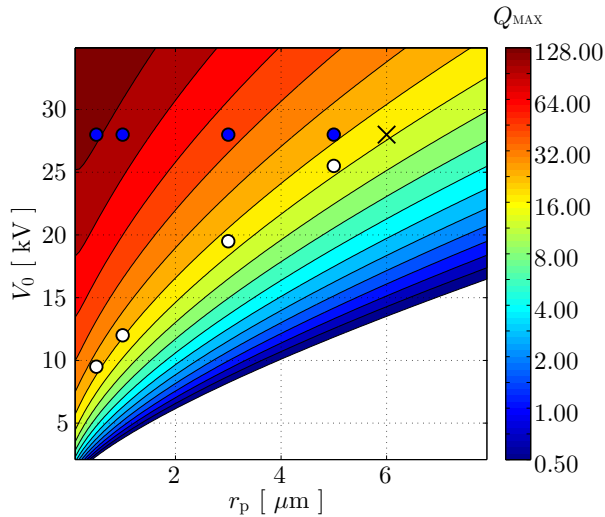
The value of Q_{MAX} according to (3.5) is plotted in fig. 4.1(a) and fig. 4.1(b), for gaps with $d = 2.5 \text{ mm}$ and $d = 5.0 \text{ mm}$, respectively. Initiation voltage as a function of tip radius has been reported by both GOURNAY AND LESAINT³ for $d = 2.5 \text{ mm}$ and YAMASHITA, YAMAZAWA, AND WANG³⁵ for $d = 5.0 \text{ mm}$. Their findings are also plotted in figs. 4.1(a) and 4.1(b). An equivalent plot for a gap size of 10 mm , which includes the point used by INGEBRIGTSEN ET AL.,⁸ is found in the appendix, fig. C.1.

Both the studies presented in fig. 4.1 agree on a critical tip radius of $r_p = 6 \mu\text{m}$ for the inception of second mode streamers, however, their propagation voltage differs by a factor of 2. This difference has a huge effect on Q_{MAX} . In fig. 4.1(a) the open points (\circ) all lie in the range $Q_{\text{MAX}} = [0.3, 2.0]$. This would imply that the electric field is too low for electron multiplication to occur according to our formulation, which assumes multiplication in the liquid phase. However, fig. 4.1(b) tells a different story. Here, the open points (\circ) lie in the range $Q_{\text{MAX}} = [18, 26]$, while the cross (\times) at $r_p = 6 \mu\text{m}$ has $Q_{\text{MAX}} = 17$. Using these values for Q_c is in line with gas theory, where $Q_c = [18, 20]$, and with the value INGEBRIGTSEN ET AL.⁸ calculated, and the values indicate that electron multiplication occurs in the liquid phase.

Interestingly enough, both the studies found a quasi-linear relation between initiation voltage for the first mode and the tip radius. The points also lie more or less on the same value of Q_{MAX} .



(a) For $d = 2.5$ mm. The plotted points are taken from GOURNAY AND LESAINT.³



(b) For $d = 5.0$ mm. The plotted points are taken from YAMASHITA, YAMAZAWA, AND WANG.³⁵

Figure 4.1: Values for Q_{MAX} as a function of needle radius and voltage, calculated according to (3.5). The solid points (●) are second mode streamers and the open points (○) are first mode streamers. The cross (x) is where the second mode intersects with the first mode.

4.1.2 Effect on the model

The variables Q_i and Q_f were introduced in section 3.3. These were the integral of α , taken from the tip to a position in the gap, and from a position in the gap to the planar electrode, respectively. Their values along the central axis are plotted in fig. 4.2. The area $Q_i > Q_c$ is where an electron avalanche can originate in order to obtain critical size. Increasing the voltage pulls this area closer to the tip. On the other hand, the area $Q_f > Q_c$ is where an electron avalanche can obtain critical size, and increasing the voltage expands this area.

For low voltages there is an area where avalanches neither can originate nor obtain maximum size, for higher voltages however, there is an overlap in the areas instead (see fig. 4.2). Lower and higher voltages are only relative measures, reducing or increasing Q_c has a similar, but opposite, effect.

Figure 4.3 illustrates how reducing Q_c increases both the area where a seed electron can originate and the area where an electron avalanche can obtain critical size. Increasing the voltage has the same effect. It is interesting to note how the area is increased, from being focused at the center, then outwards and up along the needle. This is an indicator to whether we can expect branching to occur. Branching, in our model, requires avalanches on the sides, behind the streamer head. Plots similar to figs. 4.2 and 4.3, but for higher voltages, are found in the appendix, figs. C.4 and C.5.

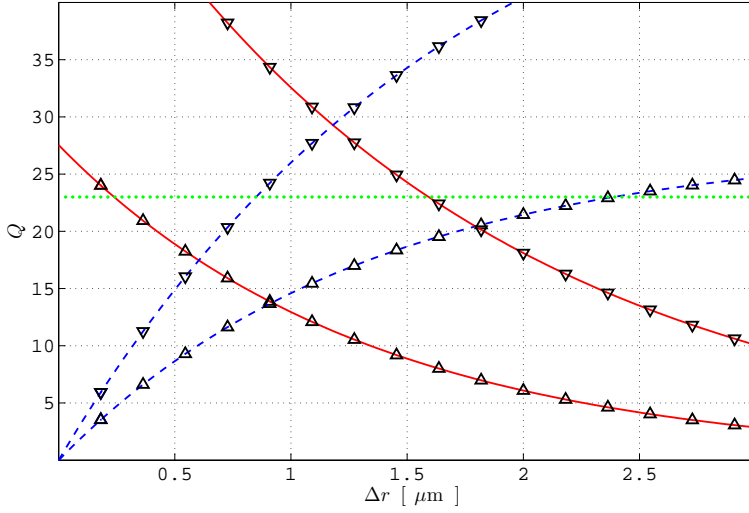


Figure 4.2: Q_i (---) and Q_f (—) are shown for $V_0 = 35$ kV (Δ) and $V_0 = 45$ kV (∇), together with $Q_c = 23$ (.....). For $d = 10$ mm and $r_p = 6.0$ μm .

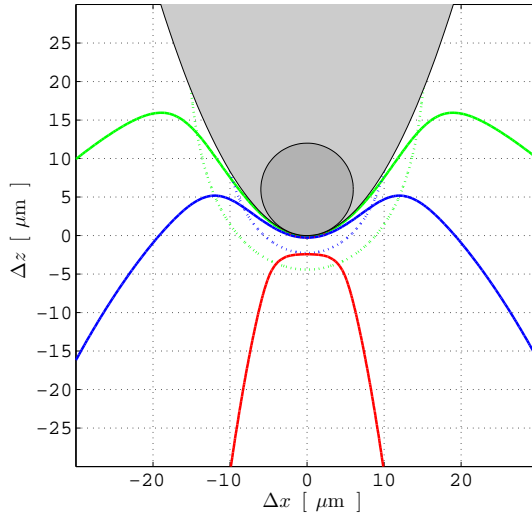


Figure 4.3: Q_i (—) and Q_f (.....) are shown for $Q_c = 23$ (—), 5 (—), and 1 (—). For $d = 10$ mm, $V_0 = 45$ kV and $r_p = 6.0$ μm . Seed electrons originating in the area below Q_i will grow into an avalanche of Q_c or larger. Electron avalanches can reach the size described by Q_c in the area above Q_f .

4.2 Photoionization model

The method for modeling photoionization from section 3.4 is presented in this section. In the first part, the field dependent photoionization cross section and the spectral radiance are plotted. This is done to verify the input to the model. In the second part, the spectral radiance and ionization rate are plotted as a function of both Δx and Δz , for chosen voltages V_0 and photon energies. The third part looks at ionization rate as a function of position and voltage, along the line $\theta = \pi$. The final part tries to evaluate the speed of propagation of the streamer, based on the ionization rate along $\theta = \pi$.

The most important plots are included in this section, and additional plots are included in appendix C.2. The plots in the appendix show the results of changing the value of parameters. There are also some additional plots enclosed, for instance how the bandwidth of cross section changes along the central line.

4.2.1 Preliminaries

The cross section is defined in (2.10) as $\sigma = \sigma_0 \sigma_\Omega \sigma_\omega$, with σ_Ω defined in (3.16), and σ_ω defined in (3.17). In general, $\sigma/\sigma_0 = \sigma_\Omega \sigma_\omega$ is referred to as the scaled cross section, as its maximum value is scaled to unity.

The scaled cross section is plotted for a number of different electrical field strengths and two different angles in fig. 4.4. Increasing the electric field strength increases the cross section for photon energies below the zero field IP, and photons traveling perpendicular to the electrical field have a higher cross section than those traveling parallel to the electric field.

In our model, the electric field strength is dependent on the position, and is strongest closest to the tip in the forward direction. For this reason the cross section is larger, and has a wider bandwidth, closer to the tip. The cross section spans to wavelengths up to about 220 nm for positions close to the streamer, and drops to about 150 nm further away.

The spectral radiance is plotted in fig. 4.5, both the initial value, and the attenuated value at a short distance from the needle. Wavelengths shorter than the radiation from the excitation peak are strongly

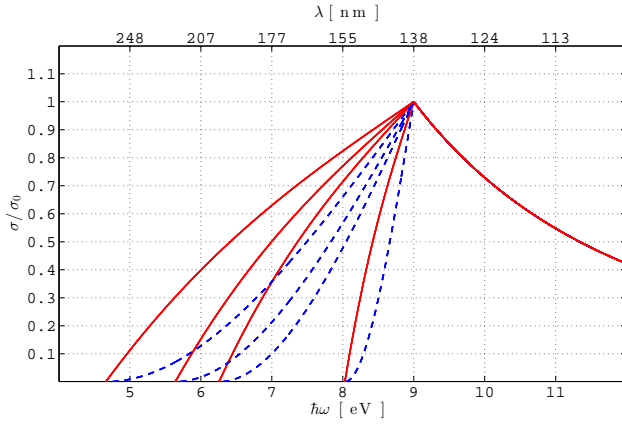


Figure 4.4: Scaled cross sections plotted as a function of photon energy, for electric field parallel (---) and perpendicular (—) to the photon momentum. The four lines are, from left to right, V_0 equal to 200 kV, 120 kV, 80 kV, and 10 kV. This corresponds to electric field strengths of 76×10^8 V/m, 45×10^8 V/m, 30×10^8 V/m, and 3.8×10^8 V/m, respectively.

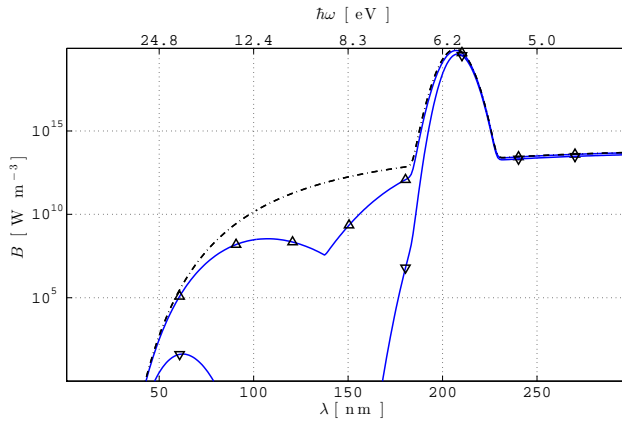


Figure 4.5: The intensity (---) of the background radiation for 7 kK combined with a peak for the first excitation energy. The two lines (—) are the intensities at a distance Δr of 10^{-7} m (Δ), and 10^{-6} m (∇).

attenuated, while the peak itself is barely affected. The reduction in radiance due to the spherical geometry is barely noticeable. The attenuation is dependent on the integral of the cross section, and the cross section's bandwidth extends to 220 nm only close to the needle. The result is that wavelengths between 190 nm to 220 nm are only a little attenuated, while wavelengths below 190 nm are more strongly attenuated.

These results are given for $V_0 = 120$ kV. Figure 4.4 shows how decreasing or increasing the voltage affects the cross section. At a voltage of 200 kV, even photon energies a little below 5 eV can be absorbed. This implies that the entire range of wavelengths in the radiation peak, to a certain degree, will be absorbed at this voltage.

4.2.2 Spatial range

Plotting the needle and surroundings in 2D is a nice way to get an overview of the situation. The situation is, however, quite complicated. We have 3 dimensions of space combined with a range of frequencies, which we want to show for different voltages, cross sections, and initial intensities.

Plotting the cross section gives some information, but it is difficult to show it properly since it changes with both V_0 and $\hbar\omega$. According to fig. 4.4, the photon energy of 6.0 eV is highly dependent on the angle between the electric field and the photon. The scaled cross section for $\hbar\omega = 6.0$ eV is plotted in figs. 4.6(a) and 4.6(b), for $V_0 = 120$ kV and $V_0 = 240$ kV, respectively. The plots give a sense of the spatial dependence of the cross section. For a voltage of 120 kV the electric field strength dominates the angular dependence, and the cross section is greatest where the electric field is strongest; directly in front of the streamer. At the higher voltage of 240 kV the cross section is still highest in the front, but the somewhat lower area also extends further out on the sides. Refer to fig. 3.2 for a plot of the electric field strength for $V_0 = 120$ kV for a comparison.

Plotting the spectral radiance is also problematic as we have to choose which photon energies and voltages to show. The spectral radiance B for $\hbar\omega = 6.0$ eV is plotted in fig. 4.7. For this energy and voltage the radiance is only attenuated close to the streamer in the forward

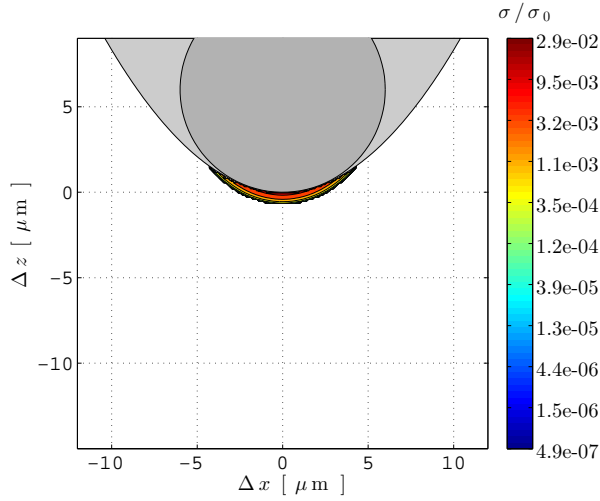
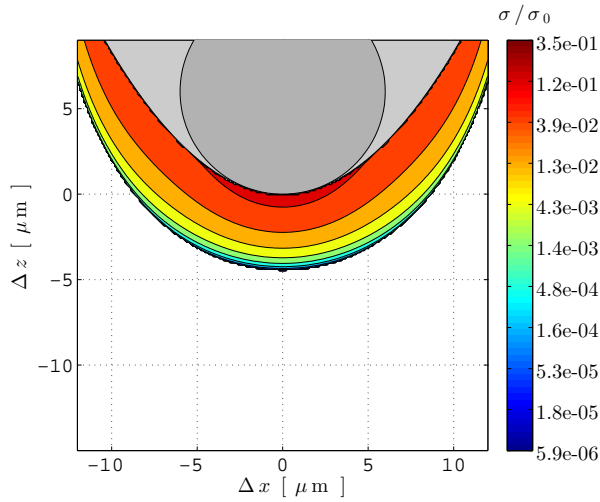
(a) $V_0 = 120 \text{ kV}$, $\hbar\omega = 6.0 \text{ eV}$.(b) $V_0 = 240 \text{ kV}$, $\hbar\omega = 6.0 \text{ eV}$.

Figure 4.6: Scaled cross section σ/σ_0 as a function of position from the needle tip. These figures illustrate how increasing the voltage increases the area where the radiation peak is able to cause ionization.

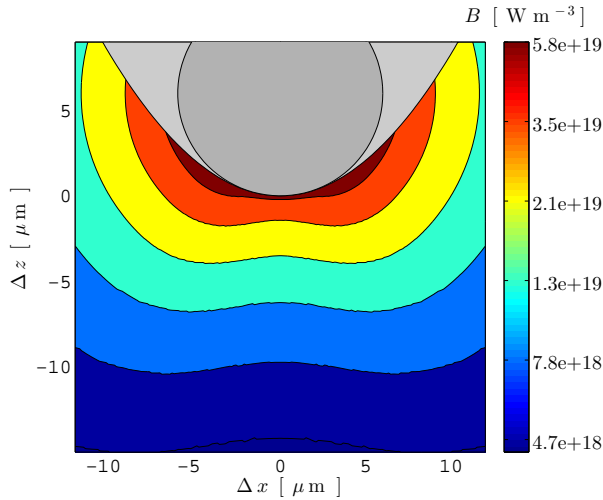


Figure 4.7: Spectral radiance B for $\hbar\omega = 6.0\text{eV}$, $V_0 = 120\text{kV}$, and $\sigma_0 = 10^{-21}\text{m}^2$. The radiance is only slightly attenuated in the forward direction.

direction, as indicated by fig. 4.6(a). For lower energies or voltages the attenuation is reduced, while for higher energies or voltages the attenuation increases in the front and begins to extend out on the sides, as indicated by fig. 4.6(b).

To find the ionization rate we integrate over all photon energies, this eliminates one variable and makes it easier to plot this rate, than to plot the cross section and the intensity. The ionization rate is plotted in fig. 4.8. Here, $\sigma_0 = 10^{-22}\text{m}^2$ has been used instead of $\sigma_0 = 10^{-21}\text{m}^2$, simply because it makes the plot more readable. By reducing the cross section by a factor of 10, both the maximum ionization and the attenuation of the intensity are reduced by a factor of 10. This makes it easier to read qualitative results.

The rate of ionization is much higher directly in front of the streamer, than on the sides. This is because this is the area with the strongest radiation and the largest cross section. The cross section is lower on the sides, but as a result, the intensity stays stronger. It is possibly the combination of these factors that makes the ionization rate more uniform at a distance from the needle.

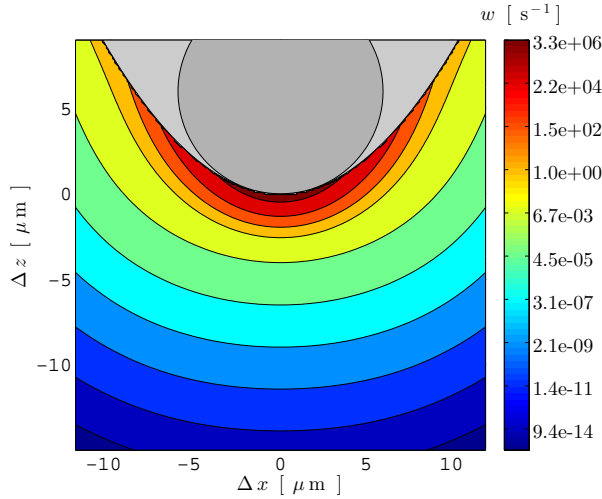


Figure 4.8: Ionization rate w for $V_0 = 120$ kV, and $\sigma_0 = 10^{-22}$ m². The highest ionization rate occurs in the forward direction, this is because the radiation peak causes ionization here. The ionization rate in other position are because of the thermal background radiation.

4.2.3 Voltage range

This section is focused on the voltage dependence of the model. The ionization rate is plotted as a function of both voltage and position, for a chosen angle θ . The central line of the hyperboloid, $\theta = \pi$, is used as a standard.

Figure 4.9 tells how increasing the voltage increases the ionization rate and extends the high ionization zone into the medium. This happens especially for voltages where the extra peak is just partly within the bandwidth of cross section. For higher voltages, the cross section for the peak is large close to the streamer, and the intensity is attenuated too much initially to cause ionization further out. Increasing the cross section increases the ionization rate closest to the streamer. It will however, also affect the attenuation of the intensity, and thus greatly reduce the affected area.

The radiation peak is responsible for the maximum ionization rate. Reducing the peak by a factor of 32, to $B_{g0} = 2.5 \times 10^{18}$ Wm⁻³, simply

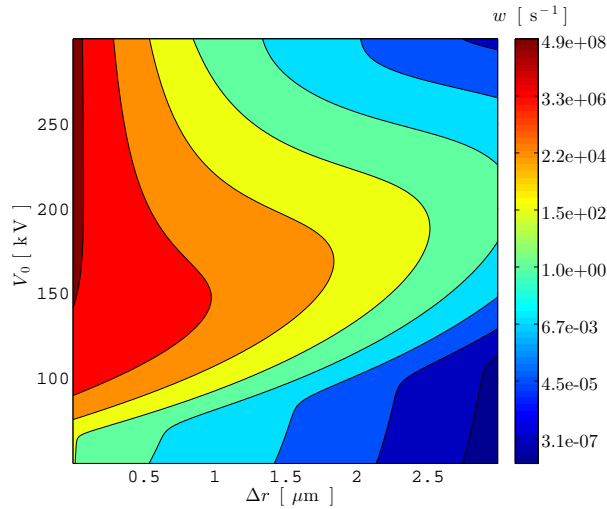


Figure 4.9: Ionization rate w , in front of the streamer at $\theta = \pi$, as a function of voltage V_0 and distance Δr from the streamer head.

reduces the maximum ionization rate by the same factor.

Both the plot for the intensity fig. 4.7 and the plot for the ionization rate fig. 4.8 indicate that the ionization rate is strongly dependent on both the distance from the needle and the angle θ . At other angles a higher voltage is required to get the electric field strong enough for the radiation peak to cause ionization. Along the central line the radiation peak falls within the bandwidth of the cross section at around 70 kV, but for $\theta = \pi/2$ this does not occur before the voltage is about 110 kV. This also implies that the voltage range where the ionization extends furthest into the liquid occurs at about 40 kV higher voltage for $\theta = \pi/2$ than for $\theta = \pi$.

4.2.4 Movement rate

The formula $v_s = \Delta r w / p$ from (3.36) provides a simple method for finding the movement rate, based on the ionization rate at a position. In fig. 4.10, the maximum value of the numerator is plotted as a function of the voltage, for the direction $\theta = \pi$, and for three different cross

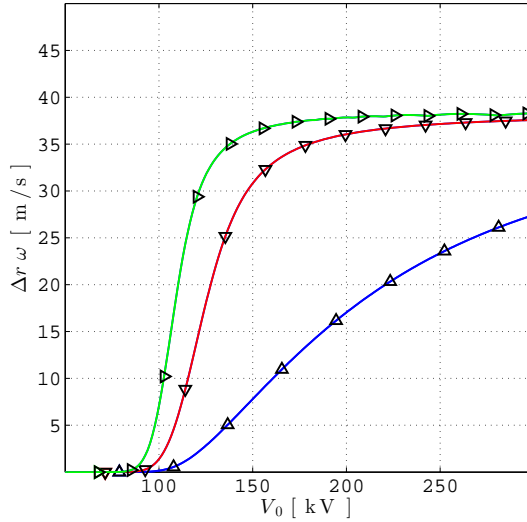


Figure 4.10: Maximum movement rate $\Delta r w$ as a function of voltage, for σ_0 equal to 10^{-22} m^2 (\triangle), 10^{-21} m^2 (∇), and 10^{-20} m^2 (\triangleright).

sections. The figure shows how a transition occurs when the voltage is high enough for the cross section's bandwidth to include the radiation peak. Increasing the cross section makes the transition occur more rapidly, but the behavior for high voltages is similar.

The rate of ionization w falls exponentially, while the distance increases linearly. As a result, the position giving the maximum movement rate is located very close to the streamer, typically within $0.1 \mu\text{m}$ to $1.0 \mu\text{m}$, depending on the cross section and voltage. For $\sigma_0 = 10^{-21} \text{ m}^2$ the maximum movement rate occurs between $\Delta r = 40 \text{ nm}$ and 200 nm . Increasing the cross section reduces these limits, and decreasing the cross section increases them. For $\sigma_0 = 10^{-22} \text{ m}^2$ the maximum Δr is $0.5 \mu\text{m}$, however, fig. 4.10 only considers a distance up to $\Delta r = 200 \text{ nm}$. As a result, the rate is actually about 15 % higher than the plotted line (\triangleleft).

The asymptotic value is linearly related to the power of the radiation peak. The curves in fig. 4.10 are plotted for a power close to 360 W , and given an ionization requirement of $p = 10^{-3}$, gives a speed of 38 km/s .

The transition from low to high movement rate occurs at higher voltage for other directions than $\theta = \pi$. This is because the electric field strength, and thus the cross section, is highest at $\theta = \pi$. The difference in angle between the electric field and the photons can only to a small degree make up for this. The movement rate at high voltages is also lower for other directions, for $\theta = \pi/2$, $\Delta r w$ has a maximum value of about 19 m/s.

Chapter 5

Discussion

5.1 The Townsend–Meek criterion

The Townsend–Meek criterion is the foundation of the present model. The Meek constant Q_c is the logarithm of the number of electrons required to create an electron avalanche of critical size.

5.1.1 Defining the Meek constant from experiments

The Meek constant $Q_c = 23$ is currently used in the model, a value calculated by INGBRIGTSEN ET AL.⁸ Data from YAMASHITA, YAMAZAWA, AND WANG³⁵ is in support of this value, while data from GOURNAY AND LESAIN³ contradicts it. The data from GOURNAY AND LESAIN indicate a value for Q_c that is so low that it contradicts the whole idea of electron avalanches in the liquid phase. This is of course, according to the current formulation, and for voltages close to the initiation voltage of the second mode.

The foundation of the present formulation is the equation for the first Townsend coefficient α found in (2.7). This equation is taken from gas discharge theory, with one modification for liquids; it is not dependent on the pressure, since the liquids are considered to be incompressible. The parameters in the formula for α , α_{MAX} and E_α , were calculated from experimental data.³⁰ The setting of these parameters, especially E_α , have a big impact on all the calculations concerning the Townsend–Meek criterion. Other experiments that can verify these parameters should be looked into. The experiments should take the time scale into account, as both charge injection³ and joule heating²⁰ can affect the result.

Regardless of the parameters α_{MAX} and E_α , there is a difference in the reported voltage thresholds. According to GOURNAY AND LESAIN

the initiation voltage of filamentary streamers is about 14.5 kV, while YAMASHITA, YAMAZAWA, AND WANG reports about 28 kV. Interestingly, INGEBRIGTSEN ET AL. finds an initiation voltage of about 14 kV,⁴⁴ and a propagation voltage of 33 kV.⁸ These differences need to be explained.

The first, and most obvious answer is that the processes investigated depend on the electric field, not directly on the voltage. The experiments mentioned above use different gap sizes d , which the magnitude of the electric field is dependent on, see (A.14). But the dependence is logarithmic, so twice the gap should not give twice the voltage.

For simplicity it was assumed that all the needle–plane electrode geometries used can be approximated by an hyperbolic needle and an infinite plane. However, YAMASHITA, YAMAZAWA, AND WANG used a needle with an apex of 20° , which makes the hyperbolic approximation a poor estimate. In addition, the use of a small planar electrode increases the initiation voltage of streamers.³ YAMASHITA, YAMAZAWA, AND WANG calculated that an electric field strength in excess of 8×10^8 V/m was required for propagation. In comparison, HAIDARA AND DENAT found a field strength of 7×10^8 V/m, and GOURNAY AND LESAINT reported a field strengths in the range 6×10^8 kV to 10^9 kV. These numbers are all in line with each other.

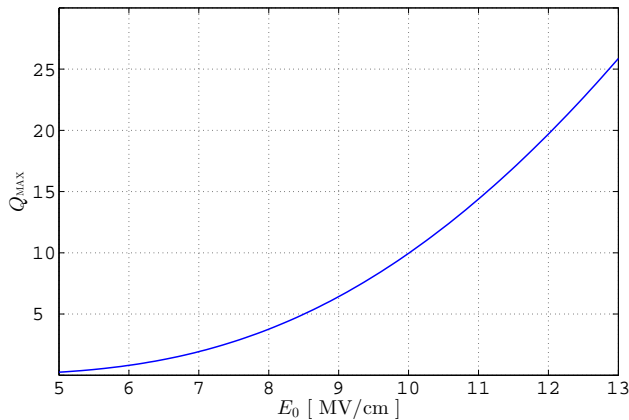


Figure 5.1: Q_{MAX} plotted against E_0 for a hyperbolic needle with tip radius $r_p = 6.0 \mu\text{m}$.

The remaining issue, however, is the propagation voltage of 33 kV used by INGBRIGTSEN ET AL., which results in a an electric field strength $E_0 = 12.5 \times 10^8$ V/m at the electrode tip. This could possibly be explained by how the various authors define and classify the streamers. YAMASHITA, YAMAZAWA, AND WANG classified the streamers as bush-like of filamentary by examining photos of the streamer development, and reported that bush-like streamers often initiated as a single filament before growing into a bush. On the other hand, GOURNAY AND LESAINTE measured the current, and used that to differentiate between streamer types. INGBRIGTSEN ET AL. also used the current to classify the streamers.

The calculations can be modified to consider the field strength instead of the gap and the voltage. With this modification, (3.5) for Q_{MAX} reads:

$$Q_{\text{MAX}} = \frac{\alpha_{\text{MAX}} E_0 r_p}{2E_\alpha} \exp\left(-\frac{B}{E_0}\right). \quad (5.1)$$

The equation is independent of d and V_0 , but still has a dependence on the needle radius r_p . However, all the research agrees on a critical needle radius of $6.0 \mu\text{m}$ for the inception of second mode streamers. The equation for Q_{MAX} is plotted for this radius in fig. 5.1. As mentioned earlier, a streamer discharge in gas is associated with an electron avalanche of the order 10^8 electrons, which equals $Q_c = 18.4$. To obtain an avalanche of the same order for cyclohexane and with a tip of radius $r_p = 6.0 \mu\text{m}$, an electric field $E_0 > 11 \times 10^8$ V/m is required. This field strength is too high when compared with the fields obtained by GOURNAY AND LESAINTE and YAMASHITA, YAMAZAWA, AND WANG, and this suggests that electron avalanches are not occurring in the liquid phase. Either the formulation, and possibly the values of α_{MAX} and E_α , has to change, or the voltage has to be much higher than the initiation voltage, in order for avalanches to occur in the liquid phase.

Changing the formulation to allow variation in the density has many consequences, for instance that E_α would be a function of the local density. A lower value for E_α would increase Q_{MAX} . Changing formulation from Laplace field to a space charge limited field (SCLF) is another possible solution.⁴⁵ Adopting a SCLF formalism implies that

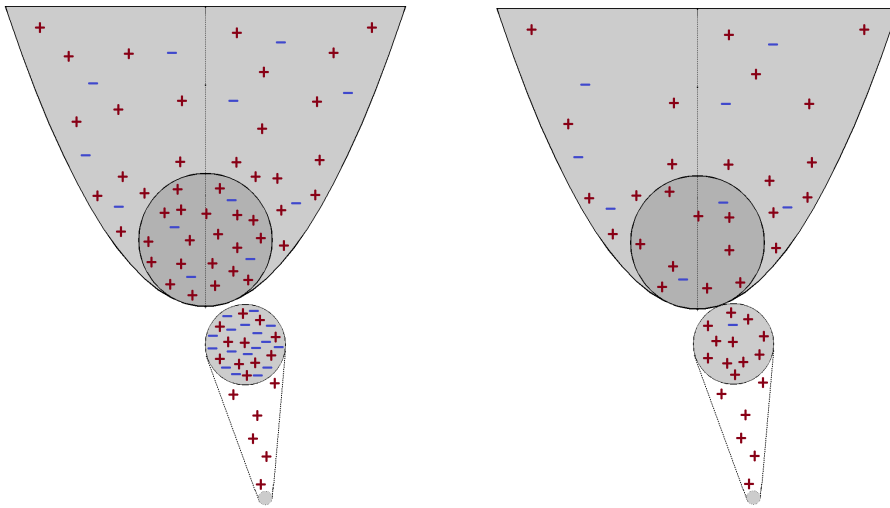
the electric field closest to the streamer is limited by space charges. This reduces the electric field strength, and thus the electron multiplication closest to the streamer. However, the SCLF enhances the electric field strength for all other areas.

5.1.2 Defining a dynamic Meek constant

The problem of the Meek constant could perhaps be viewed from another perspective, by making it a variable that depends on the electric field strength. Consider the scenario of an avalanche propagating towards the streamer head (see fig. 5.2(a)). In an area with high electric field strength, the net charge in the avalanche area is slightly negative. This is because most of the electrons are recently created, and the charge of these electrons is canceled out by the charge of newly created positive ions. The slight negative charge comes from electrons created in the tail of the avalanche. These electrons come from molecules in the tail that are now ionized. As the avalanche is propagating towards the streamer head its net negative charge increases, and so does the total positive charge in its tail as well.

These positive charges reduce the electrical field experienced by the avalanche, which reduces the propagation speed and the electron multiplication. Two things can now occur. If the effect of the tail is low, then the propagation and multiplication continues until the avalanche merges with the streamer head. The electrons of the avalanche combines with ionized molecules in the streamer head, reducing its net charge, and the positive ions left by the avalanche acts as the new tip of the streamer (see fig. 5.2(b)). If the effect of the charges in the tail is high however, then the electrons cease to multiply. This would leave a number of positive ions at a distance from the streamer, while a number of electrons, enough to cancel most of the positive charge in the streamer head, would drift to the streamer head. The ions left in the medium would then become the new streamer head. The model works by this principle, but it assumes that an avalanche stops when a critical number of electrons is reached. The electric field created by the positive ions is not explicitly considered in the model.

To get an idea of the magnitude of the electric field strength from an avalanche, we will look at the electric field created by placing all



(a) An electron avalanche that is propagating towards the streamer.

(b) A former electron avalanche that has reached the streamer or obtained critical size.

Figure 5.2: An electron avalanche before and after contact with the streamer. This is only an illustration of the principles, and the positive and negative charges have been placed just to give an impression of the net charge in the various areas.

the avalanche electrons within a sphere of $r = 6.0 \mu\text{m}$. Using $Q_c = 23$ results in an electric field strength $E_0 = 1.9 \times 10^{11} \text{ V/m}$ at the edge of the sphere, while $Q_c = 18$ results in $E_0 = 13 \times 10^8 \text{ V/m}$. The first of these field magnitudes does not make sense, it is simply too high. For this scenario, a large number of electrons from the avalanche have to stay with or recombined with their ions. The latter of the fields however, is in the correct order of magnitude.

5.1.3 Effect on the model

The variables Q_i and Q_f was defined in (3.11) and (3.12), and their values provide information on where avalanches are likely to originate and terminate, respectively. Higher value implies higher probability. The value chosen for Q_c simply decides where the probability should

be zero.

The results, namely figs. 4.2 and 4.3, indicates that avalanches are far more likely to occur in front of the streamer than on the sides. At voltages just above the propagation voltage the streamer is only able to move in the forward direction. Increasing the voltage expands the area outwards and backwards, thus the possibility for branching is increased. This is also seen in experiments, where increasing the voltage increase the number of filaments in a streamer.⁶

For the model, increasing the voltage has the same effect as reducing the Meek constant Q_c . As a result, if the Meek constant is set too high, then all the predictions of the model occurs at a voltage that is too high as well. The propagation voltage becomes too high, and higher voltage is required for branching to occur. Also, the avalanches have to come closer to the streamer before they obtain critical size, this decreases the streamer's speed. The opposite occurs if Q_c is set too low.

From figs. 4.2 and 4.3 it is seen, for high voltages, that the area where avalanches cannot originate ($Q_i < Q_c$) is located very close to the streamer. This is interesting for the next section, as it implies that seeds created by photoionization can create avalanches of critical size, even when they are created very close to the streamer.

5.2 Photoionization model

Photoionization is modeled in order to investigate the possibility of it being responsible for streamer acceleration and streamer branching. The foundation of photoionization model is the field dependent ionization cross section, in combination with a radiation peak from the streamer head.

5.2.1 Cross section

The cross section is designed to drop off for photon energies above the ionization potential. This is seen both in the definition, (3.17), of σ_ω , and in the plot of the cross section, fig. 4.4. This behavior is typical for hydrogen and other light atoms, but is not suitable for a molecule like cyclohexane. Experiments in cyclohexane show that the ionization cross section is quasi-linearly dependent on the photon energy. According to experiments, the cross section is zero for $\hbar\omega = 9.9\text{ eV}$ and increases to $5 \times 10^{-21}\text{ m}^2$ for 11.2 eV .⁴² However, it is not the energies above the IP that we are concerned with, and these numbers indicate that the cross section $\sigma_0 = 10^{-21}\text{ m}^2$ is the correct order of magnitude.

For photon energies at the first excitation energy the cross section has a strong spatial dependence (see fig. 4.6). The spatial dependence is obviously dominated by the strength of the electric field (see fig. 3.2). This is expected, since the cross section is dependent on the electrical field strength. The cross section is, however, also dependent on the angle between the electrical field and the photon momentum. The effect of this is not very visible in the results, but it is possible to see that the cross section does not follow the electric field strength perfectly.

It is total cross section that attenuates the radiation, and only the ionization cross section has been included. The total cross section also includes absorption by excitation of molecules. The absorption cross section in cyclohexane is around the first excitation energy of 7.1 eV . The first and second absorption bands have peaks at about 7.8 eV and 8.8 eV , respectively.⁴¹ Including this absorption increases the attenuation of the spectral radiance for the photon energies between the first excitation energy and the ionization potential. Photons are now

absorbed without causing ionization, this should cause the ionization rate to decrease. However, the lifetimes of the excited states is usually short, and relaxation of excited states emits photons. This way, the radiation is scattered, rather than absorbed. The effect of this is possibly increased ionization rate close to the streamer, and reduced rate further away. The actual effect on the presented model would be small since the absorption cross section is small⁴¹ at the modeled radiation peak.

Taking the absorption cross section into consideration enables us to find excitation rates. Excited molecules in the areas with high electric field strength have an increased chance of being field ionized. This mechanism would certainly increase the ionization rate in the proximity of the needle. For molecules further away, the lifetime of the excited states are probably too short for anything else than relaxation by photon emission to occur.

5.2.2 Radiation and ionization

A basis for the radiation is a spectral radiance peaked around the energy of the first electronically excited molecular state. The radiation is assumed to originate within the streamer and to only have a radial component.

Including radiation other peaks in the photoionization model is simple. Relevant candidates for this are the excited states located between the lowest state and the IP are. The resulting spectral radiance and ionization rate would simply be a superposition of all the peaks in combination with the thermal background radiation. The other peaks are assumed to be lower in magnitude, than the first peak, and as their energies are higher, they can ionize molecules at lower electric field strengths than the first peak. Consequently, fig. 4.9 would have shown higher ionization rate for the lower voltages, in the area where the first excitation cannot cause ionization.

In the previous part it was mentioned that scattering has been ignored. A mechanism that has been left out is stimulated emission. This mechanism can occur when an excited molecule is struck by a photon with energy similar to the excitation energy. The result is that the molecule relaxes, and two photons are emitted in the same direction as the original photon. This is one of the basic principles of a laser. The

effect of stimulated emission might not add up to much, but it could perhaps counter some of the scattering.

Although the possibility of radiation from the electron avalanches was mentioned in section 3.4.2 it was not included in the model. The reason for it not being included was partly that radiation from the streamer is expected to be stronger, and partly because the electric field usually is weaker around the avalanches than at the tip. The results of the model supports that a strong electric field is required for high ionization rate. The results also show that high ionization rates usually are very local. For an avalanche, local ionization just maintains its size, and this is probably already accounted for in the formula for the first Townsend coefficient.

Radiation from avalanches could be modeled with the purpose of creating new seed electrons. The seeds created in front of the avalanche, i.e. between the avalanche and the streamer, will probably not make a big difference. This is because the original avalanche is likely to obtain critical size before the newly created seeds. Nevertheless, seeds created behind the avalanche are interesting. The only problem is that the electric field strength is decreasing behind the avalanche, and this makes it less likely for photoionization to occur, especially at a distance.

The cross section depends on three factors; the photon energy, the electric field strength, and the difference in angle between the electric field and the photon momentum. One of the result we wanted for the model was to see a different behavior on the sides ($\theta \neq \pi$), since $\theta_\gamma \neq 0$ there. But according to the results the difference in electric field strength dominates. This is also seen on both the spectral radiance (see fig. 4.7) and the ionization rate (see fig. 4.8). The spectral radiance is generally attenuated close to the needle, and mainly in the forward direction. This is again reflected on the ionization rate, which also is strongest in the forward direction, but only close to the needle. A few μm away from the needle is the ionization rate similar for all directions, even for higher voltages.

The density is viewed as constant in the present model. Allowing the density to change has many implications. For the spectral radiation a change in the density affect the attenuation the same way a change in

the cross section does; reduced density results in reduced attenuation. Higher radiation results in higher ionization rate w (except at the needle interface), and extends the high ionization rate area. This is of course with regards to the ionization rate per atom w , not the ionization rate per volume W .

5.2.3 Movement rate

The main objective of the photoionization model is to predict the streamer speed for fast streamers. The results show a transition from zero to a constant movement rate over a range of about 50 kV. The movement rate is linearly dependent on both the ionization requirement p , and the radiated power $P \sim B_{g0} \Delta\lambda$. The values used in the model was more or less arbitrarily chosen in order to get a result in the correct order of magnitude.

A degree of ionization $p = 10^{-3}$ has been reported,⁸ but this is within the streamer, not in front of the streamer. The density within the streamer is lower than in front of the streamer,⁴ so using $p = 10^{-3}$ might not be appropriate. However, the assumptions done in the end of section 5.1.2, where all the ions left by an avalanche enclosed within a sphere of $r = 6.0 \mu\text{m}$, can be applied here as well. For $Q_c = 23$, $p = 1.1 \times 10^{-4}$, and for $Q_c = 18$, $p = 7.3 \times 10^{-7}$. These numbers suggest that using $p = 10^{-3}$ is conservative, and that the speed could be higher than indicated by the results. However, the chosen power might be too high, and reducing the power would result in a lower speed.

The power of the first excitation peak is about 363 W. GOURNAY AND LESAIN⁵ found the power of the streamer head by calculating the thermal vaporization energy required per unit length of streamer. Multiplying this number with the speed gives the power, which was 10 W for the slow streamers considered in their article. The calculated energy for streamer creation was about 4×10^{-3} J/m, and was for pentane. Using the same number as an approximation yields a speed of 91 km/s, which is the same order of magnitude as the model. This is of course just a rough estimate, but the speed indicates that the power is within the correct order of magnitude.¹⁸

Setting the power constant, while changing the applied voltage is a grave simplification. The power is likely to change, and be dependent

on several factors. Increasing the voltage should increase the power. However, unless the voltage dependence is very strong, the result would still be a low movement rate for low voltages, followed by a transition for higher voltages. The difference is that the movement rate would no longer be constant for voltages above the transition.

It is evident that there are some pieces missing for the model to correctly predict the magnitude of the streamer propagation speed. Still, the transition in movement rate is interesting. The transition occurs when the IP is reduced to the first excitation energy by a strong electric field. With the chosen parameters the transition begins at about $V_0 = 100$ kV (see (— \blacktriangle) in fig. 4.10). In a gap of $d = 50$ mm this occurs at $V_0 = 120$ kV, which is the value found by LESAINTE AND JUNG.¹⁸ LINHJELL ET AL.⁴⁶ also found an acceleration voltage of 120 kV, but for a gap of $d = 88$ mm. Increasing the gap from 50 mm to 77 mm does not have a big impact on the model, which is only dependent on the logarithm of d . However,⁴⁷ finds an acceleration voltage of on 58 kV for a gap of $d = 5$ mm. The model is not able to reproduce this, and indicates about 90 kV as acceleration voltage for this gap size. This could indicate that either the model just coincidentally found the correct voltage for the large gaps, or that another mechanism is responsible for the acceleration in small gaps.

5.2.4 Potential seeds

Electrons created by photoionization can be considered as new seeds for electron avalanches. In the front of the streamer, this could act as a feed-forward mechanism, which increases the speed of the streamer. On the side of the streamer, an increased number of seeds could increase the probability of streamer branching.

In section 4.1 the Townsend–Meek criterion was discussed. The results showed that seeds created in an area close to the streamer are not able to obtain critical size. However, increasing the voltage or decreasing the critical size Q_c decreased this area. This is better seen in fig. 5.3, where $Q_i = Q_c$ has been plotted along the central line.

The results showed that photoionization occurred very close to the streamer. Figure 5.3 indicates that even the seeds created really close can obtain critical size. The area where $Q_i > Q_c$ has a strong

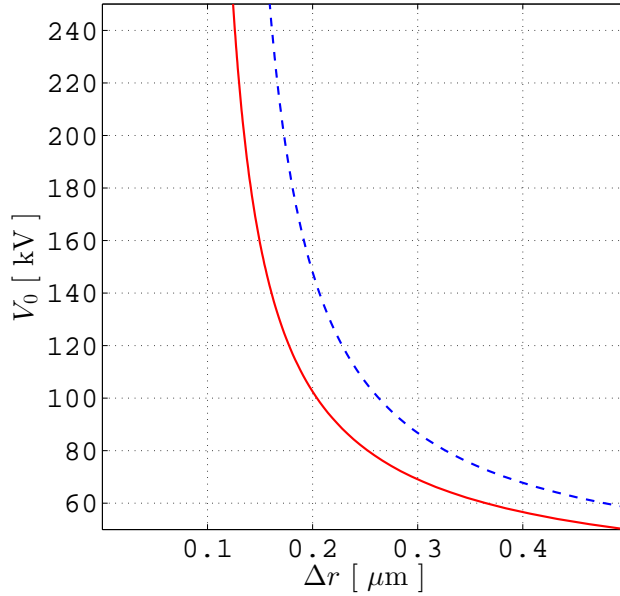


Figure 5.3: The distance from the needle where $Q_i = Q_c$, plotted against V_0 for $Q_c = 18$ (—), and $Q_c = 23$ (---), along the central line, $\theta = \pi$, in a gap of $d = 10$ mm, and a needle $r_p = 6.0$ μm . Seed electrons originating to the left of these lines cannot multiply into an avalanche of critical size Q_c .

dependence on the voltage below about 100 kV, and a much weaker dependence on the voltage above this threshold. This is a very interesting detail. The results (specifically fig. 4.9) showed that the area of high ionization rate increased for a range of voltages above 100 kV.

Combining the increase of $Q_i > Q_c$ with increased ionization rate could provide the extra seeds required for a speed transition to the fourth mode. The situation is of course not as simple as the impression given above. A seed originating at $Q_i = Q_c$ obtains critical size at $\Delta r = 0$, and will not add any speed to the model. In addition, at a speed of 100 km/s the streamer moves a distance $\Delta r = 0.1$ μm in 10^{-12} s. This makes it more difficult for the seeds to obtain critical size.

The value of Q_i is dependent on the electric field strength, not directly on the voltage. As such, a plot of $Q_i = Q_c$ for other directions would show similar trends as fig. 5.3, but occurring at higher voltages.

The results showed that the high ionization area became smaller at very high voltages. This is because most of the radiation is absorbed close to the streamer. These results show that at a certain range of high voltages the ionization becomes more local in front of the streamer, while it becomes less local at the sides, e.g. $\theta = \pi/2$. This implies that for certain voltages more seeds are created on the sides than in the front of the streamer.

5.3 Implementing photoionization

The whole model for photoionization can easily be implemented into the existing model for streamer propagation. The only thing missing is to find the correct magnitude for certain parameters, in particular; the power P of the radiation peak and the ionization requirement p .

The movement rate $v_s = \Delta r w/p$ can be treated as the background speed of the streamer. This way, the minimum movement of the streamer is $v_s \Delta t$. Avalanches obtaining critical size can increase this movement, but not reduce it.

New seeds can be added according to a Monte Carlo scheme. The probability of creating a seed electron within a small volume \mathcal{V} with the ionization rate W is:

$$P(\text{CREATION}) = \mathcal{V}W\Delta t, \quad (5.2)$$

where Δt is the time step of the model.

Even though implementing the model this way is easy, it is not particularly clever. The present model is built to be fast, and is founded on simple principles. For the photoionization model presented here, however, the calculation time required to plot a realization of fig. 4.8 was about one hour, when using 12 CPU cores on a computation server. This is unacceptable for the final model, a more efficient approach is required.

The movement rate v_s depends only on the conditions very close to the streamer head. This makes it possible to ignore the electric field from other streamer heads. The only variables left to consider is the gap distance and the potential of the streamer head. By calculating v_s in advance, for a range of gap distances and voltages, the required

computation time is considerably reduced because we can now find the value in a table.

It is more difficult to find an easy solution for the creation of new seeds. The relevant areas for creation of seeds are at a distance from the streamer head, and the electric field from other heads may have to be considered. This would make it impossible to perform generic calculations in advance, but generic calculations may still provide a good approximation.

The huge time consumption used to produce the plots within this thesis was required for the integration of the cross section, which was usually done for 200×200 positions for 500 photon energies. This can obviously be done more efficiently if we know where to look and what to calculate. Using a Monte Carlo scheme can also reduce the amount of calculations required.

In a Monte Carlo scheme we would limit the radiation to a given number of random directions. The cross section would then only have to be integrated for these few directions, which saves a lot of calculation time. Then the same scheme as proposed earlier for creation of seed electrons can be employed.

Chapter 6

Conclusion

In this thesis we have explored the foundation of SINTEF's streamer model and proposed a novel model for photoionization.

6.1 The Townsend–Meek criterion

The foundation of the model is the Townsend–Meek criterion, with the Meek constant $Q_c = 23$ as the most important parameter. This value was calculated by INGBRIGTSEN ET AL.⁸ Values for Q_c calculated from data available in literature were much lower than the value currently used in the model. Data from GOURNAY AND LESAIN³ indicated a value for Q_c close to 1, and data from YAMASHITA, YAMAZAWA, AND WANG³⁵ indicated $Q_c = 17$ for a tip of critical size. The hyperbolic approximation that was used for the calculations. This method is, however, not very accurate for the latter of these studies.

The propagation voltage of the present model is too high. A reduction in Q_c will reduce the propagation voltage, however, the value $Q_c = 1$ is so low that it contradicts the whole idea of critical electron avalanches in liquid phase.

The difference in the results is probably caused by the methods used to characterize the streamers. Pictures give different results than measuring the current, and characterizing a streamer at the initiation can give a different result than characterizing a developed streamer. The exact characterization of a propagating second mode streamer needs to be decided. This is a necessity before the Meek constant Q_c can be found experimentally.

6.2 Photoionization

Photoionization could play a role in the mechanisms of both the third-/fourth streamer mode and streamer branching. The proposed model is based on two main principles. The first of which is that the radiation is dominated by a peak around the first excitation energy. The second is the assumption that a field dependent reduction in the ionization potential increases the bandwidth of the ionization cross section. The results show that the ionization rate is dominated by the electric field strength, which is strongest in front of the streamer.

Many of the parameters for the model are not known, and as such, approximate values or best guesses are used as input. Nevertheless, the model correctly predicts a transition in the speed. The transition occurs when the field dependent ionization potential is reduced to the level of the first excitation energy.

The model shows how the ionization rate increases and the high ionization zone expands outwards from the streamer, for the range of voltages where the cross section for the radiation peak is low. For higher voltages, the cross section becomes high close to the streamer. This increases the ionization rate close to the streamer, but also reduces the size of the high ionization zone. According to this mechanism, at certain high voltages, the high ionization zone extends further on the sides of the streamer than in the front. The ionization rate is nevertheless, always highest in front of the streamer.

Photoionization is a very local process, at least according to this model. However, a closer look at the Townsend–Meek criteria revealed that seeds very close to the streamer can obtain critical size, as long as the voltage is high. These results, in combination with the behavior of the high ionization zone, suggest that above a threshold voltage, photoionization begins to generate seeds in front of the streamer. Increasing the voltage makes the photoionization more localized in front of the streamer. This increases the ionization rate, but reduces the generation of potential seeds. On the other hand, increasing the voltage increases the size of the high ionization zone on the sides of the streamer. This increases the generation of seeds there. Seeds produced in front of the streamer may increase the speed of the streamer, while seeds produced on the sides may increase the probability of streamer

branching.

In conclusion, the photoionization model seems promising. Especially since it predicts the correct voltage for transition from a slow to a fast speed. However, the model needs to be tested for other cases as well to ensure that this is a fact, rather than a coincidence. The model is also promising with regards to production of seed electrons, but this as well needs to be looked at more thoroughly.

Appendix A

Prolate spheroidal coordinates

A.1 Basic properties

The Laplace equation for a hyperbolic needle above a plane is separable in prolate spheroidal coordinates. This fact makes these our preferred coordinates when looking into electrical properties. The basis for this coordinate system is a series of ellipsoids and hyperboloids with rotational symmetry about an axis. We will use the convention where the Cartesian coordinates are defined as:

$$x = a \sinh \mu \sin \nu \cos \phi, \quad (\text{A.1})$$

$$y = a \sinh \mu \sin \nu \sin \phi, \quad (\text{A.2})$$

$$z = a \cosh \mu \cos \nu. \quad (\text{A.3})$$

Here μ is a nonnegative real number defining the ellipsoids, $\nu \in [0, \pi]$ is the latitude and gives the asymptotic behavior of hyperboloids, and $\phi \in [0, 2\pi]$ is the azimuthal angle. The system is shown in fig. A.1. Changing from Cartesian to prolate spheroidal coordinates is performed by using:

$$\mu = \operatorname{acosh} \left\{ \frac{1}{2a} \sqrt{x^2 + y^2 + (z+a)^2} + \frac{1}{2a} \sqrt{x^2 + y^2 + (z-a)^2} \right\}, \quad (\text{A.4})$$

$$\nu = \operatorname{acos} \left\{ \frac{1}{2a} \sqrt{x^2 + y^2 + (z+a)^2} - \frac{1}{2a} \sqrt{x^2 + y^2 + (z-a)^2} \right\}, \quad (\text{A.5})$$

$$\phi = \operatorname{atan} \left\{ \frac{y}{x} \right\}. \quad (\text{A.6})$$

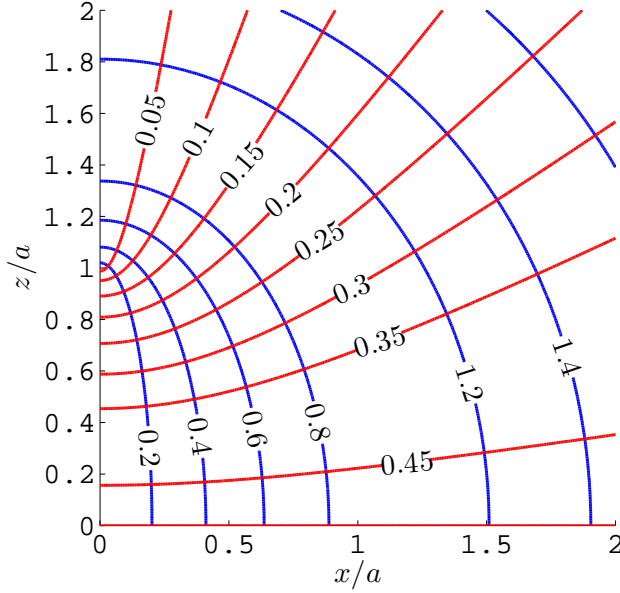


Figure A.1: Definition of the prolate spheroid coordinate system (μ, ν, ϕ) , the hyperboles (—) are lines of constant ν and the ellipsoids (—) are lines of constant μ . Here, ν is given in units of π . The azimuthal angle ϕ , which gives the rotation about the z -axis, is not shown here.

The ellipsoids are defined by a constant μ , and are obtained by:

$$z(x, y, \mu) = a \cosh \mu \left(1 - \frac{x^2 + y^2}{a^2 \sinh^2 \mu} \right)^{1/2}. \quad (\text{A.7})$$

While the hyperboles, which are defined by a constant ν , are obtained by:

$$z(x, y, \nu) = a \cos \nu \left(1 + \frac{x^2 + y^2}{a^2 \sin^2 \nu} \right)^{1/2}. \quad (\text{A.8})$$

We will see that the electrical potential is defined by ν while the electrical field flux follow constant μ lines.

The needle hyperbola is defined by ν_0 . For a sharp tip $r_p \ll a$, we can assume that $\nu_0 \ll 1$, and use the approximation:

$$\cos\left\{\nu(0, 0, z = d)\right\} = d/a \approx 1 - \nu_0^2/2. \quad (\text{A.9})$$

Solving for ν_0 gives:

$$\nu_0 \approx \sqrt{r_p/d}. \quad (\text{A.10})$$

We also have:

$$\hat{\nu} = \frac{x \hat{x} + y \hat{y} - z \tan^2 \nu \hat{z}}{a \sin \nu \left(\sinh^2 \mu + \cosh^2 \mu \tan^2 \nu \right)^{1/2}}, \quad (\text{A.11})$$

and for integration $\hat{\nu}$ we use:

$$\begin{aligned} d\ell &= \left(dx^2 + dy^2 + dz^2 \right)^{1/2} \\ &= \left(\left(\frac{dx}{d\nu} \right)^2 + \left(\frac{dy}{d\nu} \right)^2 + \left(\frac{dz}{d\nu} \right)^2 \right)^{1/2} d\nu \\ &= a \left(\sinh^2 \mu \cos^2 \nu + \cosh^2 \mu \sin^2 \nu \right)^{1/2} d\nu. \end{aligned} \quad (\text{A.12})$$

A.2 Electrical properties

Prolate spheroid coordinates are preferable as the Laplace equation is separable, and thus easy to solve. The potential is turns out to be only dependent on ν and is found by solving $\nabla^2 V = 0$:

$$V(\nu) = C \ln \cot(\nu/2). \quad (\text{A.13})$$

The constant C is defined by the potential at the needle:

$$C = \frac{V_0}{\ln \cot(\nu_0/2)} \approx \frac{2V_0}{\ln(4d/r_p)}. \quad (\text{A.14})$$

The electrical field is found by differentiating the potential:

$$E(\mu, \nu) = -\nabla V = \frac{C}{a \sin \nu (\cosh^2 \mu - \cos^2 \nu)^{1/2}}, \quad (\text{A.15})$$

with $E = E \hat{\nu}$. The electric field close to the needle is plotted in fig. 3.2. Along the central line (A.15) is reduced to:

$$E(0, \nu) = \frac{C}{a \sin^2 \nu}, \quad E(0, 0, z < a) = \frac{aC}{a^2 - z^2}. \quad (\text{A.16})$$

Integration of (A.16) yields the potential along the same line:

$$V(0, 0, z < a) = \frac{C}{2} \ln \left(\frac{a+z}{a-z} \right). \quad (\text{A.17})$$

It is easy to confirm that inserting $V = V_0$ at $z = d$ gives the same value for C as (A.14) as long as $r_p \ll d$. By letting $r = a - z$, $r \ll a$ and $x = y = 0$ we can also use:

$$E(r) = \frac{C}{r_p} \frac{r_0}{r} = E_0 \frac{r_0}{r}, \quad (\text{A.18})$$

and

$$V(r) = \frac{C}{2} \ln \left(\frac{2d}{r} \right). \quad (\text{A.19})$$

These are good approximations for the area close to the needle, which is the area we are interested in, but they only hold along the center line. For other positions we have to use the full expressions.

Appendix B

Calculations

This section contains the detailed calculation of (3.15):

$$\sigma_{\Omega} = C_{\Omega} \int_0^{2\pi} \int_0^{\Theta} \sin^2(\theta_{\gamma} - \theta_e) \sin \theta_e d\theta_e d\phi, \quad (\text{B.1})$$

which results in equation (3.16). Refer to fig. 3.4 for an overview of the variables.

We start by finding the normalization constant C_{Ω} , for the case when $\theta_{\gamma} = 0$ and $\Theta = \pi/2$:

$$1 \equiv C_{\Omega} \int_0^{2\pi} \int_0^{\pi/2} \sin^2 \theta_e \sin \theta_e d\theta_e d\phi = C_{\Omega} 2\pi \frac{2}{3}, \quad (\text{B.2})$$

which gives:

$$C_{\Omega} = \frac{3}{4\pi}. \quad (\text{B.3})$$

For this calculation, and others to come it is convenient to have the relations:

$$\int \cos^2 t \sin t dt = -\frac{1}{3} \cos^3 t, \quad (\text{B.4})$$

$$\int \sin^3 t dt = \int (1 - \cos^2 t) \sin t dt = -\cos t + \frac{1}{3} \cos^3 t, \quad (\text{B.5})$$

$$\int_0^{2\pi} \sin^2 t dt = \int_0^{2\pi} \cos^2 t dt = \pi. \quad (\text{B.6})$$

For the case when $\theta_\gamma = 0$ we can write:

$$\sigma_\Omega = \frac{3}{4\pi} \int_0^{2\pi} \int_0^\Theta \sin^2 \theta_e \, d\Omega = \frac{3}{4\pi} \int_0^{2\pi} \int_0^\Theta \frac{x^2 + y^2}{r^2} \, d\Omega. \quad (\text{B.7})$$

The angle θ_γ lies in the xz -plane. Introducing this angle is the same as rotating our coordinate system. After the rotation we have:

$$\sigma_\Omega = \frac{3}{4\pi} \int_0^{2\pi} \int_0^\Theta \frac{(x \cos \theta_\gamma - z \sin \theta_\gamma)^2 + y^2}{r^2} \, d\Omega. \quad (\text{B.8})$$

The system is now oriented according to the electric field, with $E = E\hat{z}$. The equation would have looked simpler if we had rotated the electrical field instead, but this method implies that the limits of θ and ϕ both change, which makes integration hard to do. Each term of the integral is easily solved:

$$\begin{aligned} \int \frac{x^2}{r^2} d\Omega &= \int (\sin \theta \cos \phi)^2 \sin \theta \, d\theta \, d\phi \\ &= \int_0^{2\pi} \cos^2 \phi \, d\phi \cdot \int \sin^3 \theta \, d\theta \\ &= \frac{\pi}{3} (-3 \cos \theta + \cos^3 \theta), \end{aligned} \quad (\text{B.9})$$

$$\begin{aligned} \int \frac{y^2}{r^2} d\Omega &= \int (\sin \theta \sin \phi)^2 \sin \theta \, d\theta \, d\phi \\ &= \int_0^{2\pi} \sin^2 \phi \, d\phi \cdot \int \sin^3 \theta \, d\theta \\ &= \frac{\pi}{3} (-3 \cos \theta + \cos^3 \theta), \end{aligned} \quad (\text{B.10})$$

$$\begin{aligned} \int \frac{z^2}{r^2} d\Omega &= \int (\cos \theta)^2 \sin \theta \, d\theta \, d\phi \\ &= \int_0^{2\pi} d\phi \cdot \int \cos^2 \theta \sin \theta \, d\theta \\ &= -\frac{2\pi}{3} \cos^3 \theta, \end{aligned} \quad (\text{B.11})$$

$$\begin{aligned}
\int \frac{xz}{r^2} d\Omega &= \int \sin \theta \cos \phi \cdot \cos \theta \sin \theta d\theta d\phi \\
&= \int \cos \phi d\phi \cdot \int \sin^2 \theta \cos \theta d\theta \\
&= 0.
\end{aligned} \tag{B.12}$$

This is all the input needed to calculate the integral for the cross section,

$$\begin{aligned}
\sigma_{\Omega} &= \frac{3}{4\pi} \int_0^{\Theta} r^{-2} \left\{ (x \cos \theta_{\gamma} - z \sin \theta_{\gamma})^2 + y^2 \right\} d\Omega \\
&= \frac{3}{4\pi} \int_0^{\Theta} \left\{ (1 + \cos^2 \theta_{\gamma}) \frac{x^2}{r^2} + \sin^2 \theta_{\gamma} \frac{z^2}{r^2} \right\} d\Omega \\
&= \left[\frac{1}{4} (1 + \cos^2 \theta_{\gamma}) (-3 \cos \theta + \cos^3 \theta) - \frac{1}{2} \sin^2 \theta_{\gamma} \cos^3 \theta \right]_0^{\Theta} \\
&= \frac{1}{4} (1 + \cos^2 \theta_{\gamma}) (\cos^3 \Theta - 3 \cos \Theta + 2) - \frac{1}{2} \sin^2 \theta_{\gamma} (\cos^3 \Theta - 1) \\
&= 1 - \frac{1}{4} (1 + \cos^2 \theta_{\gamma}) (3 \cos \Theta - \cos^3 \Theta) - \frac{1}{2} \sin^2 \theta_{\gamma} \cos^3 \Theta. \tag{B.13}
\end{aligned}$$

The expression equals zero when $\Theta = 0$, and equals unity when $\theta = \pi/2$. The value between these two states depends on the angle between the photon and the electric field θ_{γ} .

Appendix C

Additional plots

The most important and descriptive plots were included in the results, chapter 4. This appendix contains additional plots and information. The importance of a figure is briefly given in its description, but it is assumed that chapter 4 has already been read. The section names used here matches the relevant section of the results.

C.1 The Townsend–Meek criterion

C.1.1 Finding the Meek constant

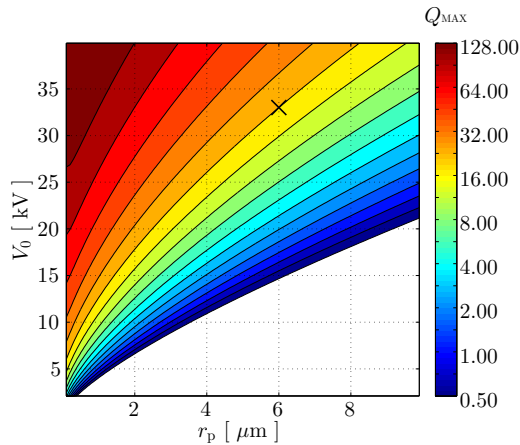
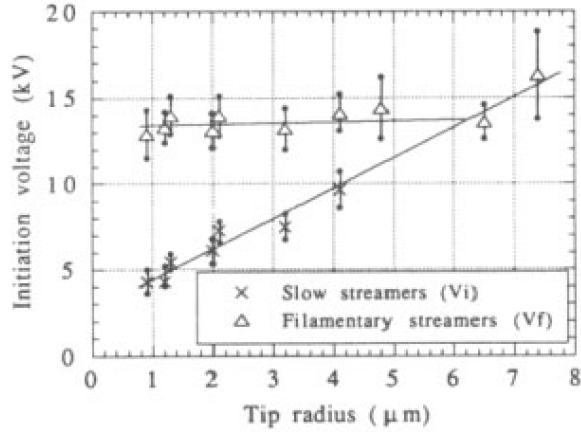
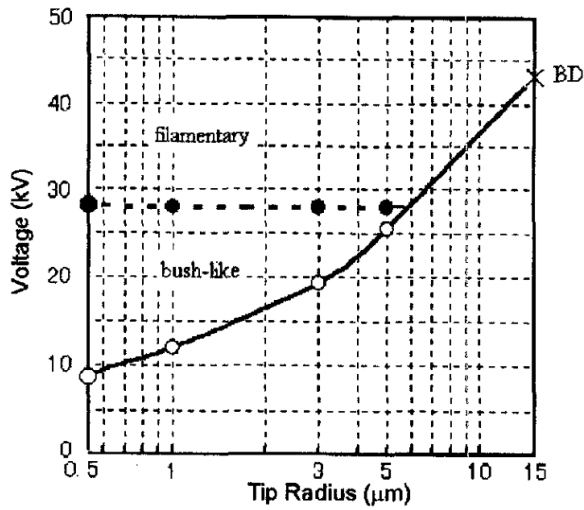


Figure C.1: Values for Q_{MAX} as a function of needle radius and voltage, calculated according to (3.5), for $d = 10 \text{ mm}$. The cross (x) is the point calculated by INGEBRIGTSEN ET AL.⁸ Similar plots for $d = 2.5 \text{ mm}$ and $d = 5.0 \text{ mm}$ are found in figs. 4.1(a) and 4.1(b).



r_p	V_0	Q_{MAX}	r_p	V_0	Q_{MAX}
0.8	4.3	2.0	0.8	13.0	37.2
1.2	4.3	0.7	1.2	13.2	28.5
1.2	5.5	2.0	1.2	13.4	28.5
2.0	6.0	0.7	2.0	14.0	17.2
2.0	7.3	1.6	2.0	13.0	14.3
3.2	7.2	0.3	3.2	13.3	6.0
4.0	9.6	0.6	4.0	14.0	4.1
6.4	13.6	0.7	4.8	14.2	2.6
7.4	16.6	1.2			

Figure C.2: The plot is fig. 10 from GOURNAY AND LESAINT,³ which gives the variation of the initiation voltage as a function of tip radius, for a gap of 2.5 mm. The table on the left are values read from the points following the tilted line, while the table on the right are values read from points following the constant line. Q_{MAX} is calculated according to the approximation given in (3.5). These are the points plotted in fig. 4.1(a).



r_p	V_0	Q_{MAX}
0.5	28.0	132.6
1.0	28.0	110.9
3.0	28.0	51.5
5.0	28.0	24.4
0.5	9.5	25.9
1.0	12.0	23.4
3.0	19.5	19.4
5.0	25.5	17.9
6.0	28.0	17.0
15.0	43.0	9.2

Figure C.3: The plot is fig. 14 from YAMASHITA, YAMAZAWA, AND WANG,³⁵ which gives the variation of the initiation voltage as a function of tip radius, for a gap of 5.0 mm. The first section are values read from the solid points, middle section are values read from the open points, and the third section contains the interpolated critical tip value and the breakdown value. Q_{MAX} is calculated according to the approximation given in (3.5). These are the points plotted in fig. 4.1(b).

C.1.2 Effect on the model

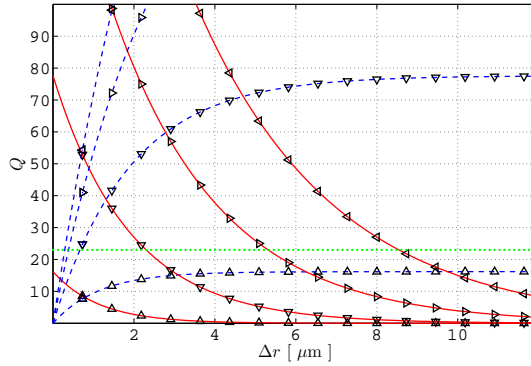


Figure C.4: Q_i (---) and Q_f (—) are shown for various values of V_0 : 30 kV (Δ), 50 kV (∇), 70 kV (\triangleright), and 90 kV (\triangleleft), together with $Q_c = 23$ (- - -). For $d = 10\text{ mm}$ and $r_p = 6\text{ }\mu\text{m}$. This plot is similar to fig. 4.2, but shows a wider range of voltages for a longer distance Δr . Q_i (---) indicates that even avalanches initiating very close to the streamer ($\Delta r < 1\text{ }\mu\text{m}$) may obtain critical size. Q_f (—) indicates how increasing the voltage makes it possible for an avalanche to obtain critical size further away. At 90 kV, critical size may be obtained over $8\text{ }\mu\text{m}$ from the tip.

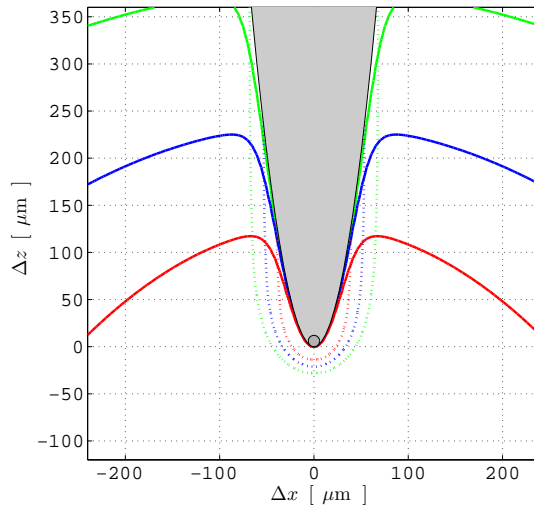


Figure C.5: Q_i (—) and Q_f (· · ·) are shown for $Q_c = 23$ (—), 5 (—), and 1 (—). For $d = 10$ mm, $V_0 = 120$ kV and $r_p = 6$ μm . This plot is similar to fig. 4.3, but is for a higher voltage and a wider area. The plot indicates how a reduction in Q_c increases both the area where an avalanche can obtain critical size (above · · ·) and the area where an avalanche may originate in order to obtain critical size (below —). This figure gives a good impression of how likely branching is to occur.

C.2 Photoionization model

C.2.1 Preliminaries

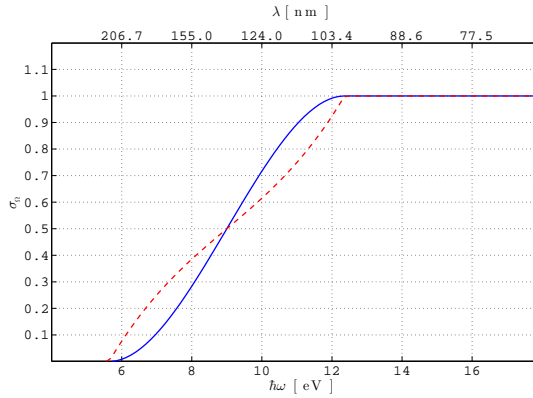


Figure C.6: This is a plot of σ_{Ω} where $\Theta \in [0, \pi]$, for $V_0 = 120$ kV, with the electric field parallel (---), and perpendicular (—) to the photon momentum. For $V_0 = 0$ kV the plot would be a step function at $h\omega = 9.0$ eV. With this formulation, applying an electric field increases the cross section for photon energies below the IP, and reduces the cross section for photon energies above the IP.

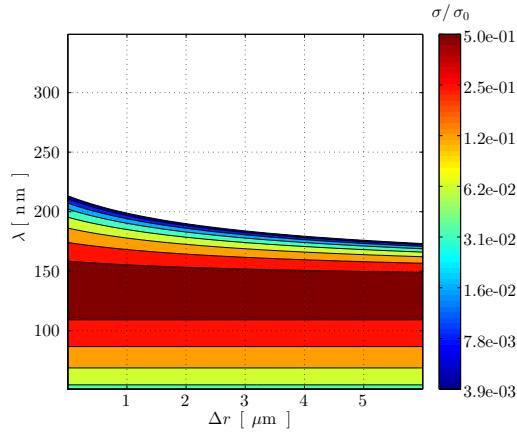


Figure C.7: Scaled cross section, σ/σ_0 . The cross section's dependence on wavelength and position, for $\theta = \pi$, and $V_0 = 120$ kV. This type of plot is not included in the results section, but it gives some of the same information as ???. The electric field is strongest close to the needle, this makes the bandwidth of the cross section widest here. As the electric field strength is reduced, so is the bandwidth of the cross section.

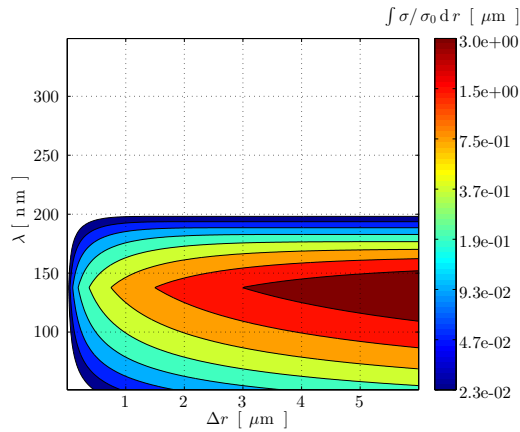


Figure C.8: Scaled cross section, σ/σ_0 , integrated from the tip. The cross section's dependence on wavelength and position, for $\theta = \pi$, and $V_0 = 120$ kV.

C.2.2 Spatial range

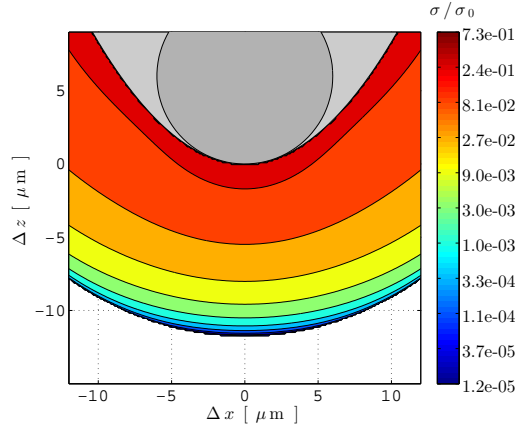
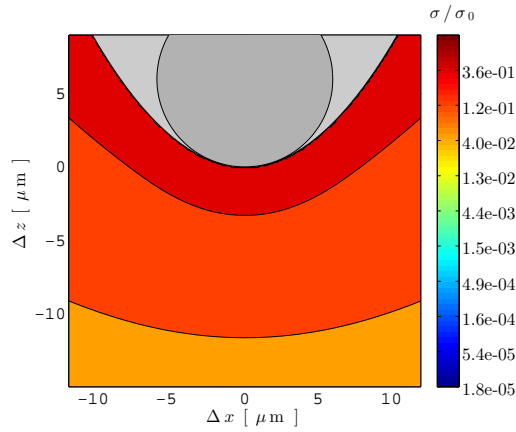
(a) $V_0 = 120 \text{ kV}$, $\hbar\omega = 7.5 \text{ eV}$.(b) $V_0 = 240 \text{ kV}$, $\hbar\omega = 7.5 \text{ eV}$.

Figure C.9: Scaled cross section σ/σ_0 as a function of position from the needle. These figures are similar to figs. 4.6(a) and 4.6(b), which are plotted for $\hbar\omega = 6.0 \text{ eV}$. The plots indicate that considering an increased voltage is qualitatively the same as considering a higher photon energy.

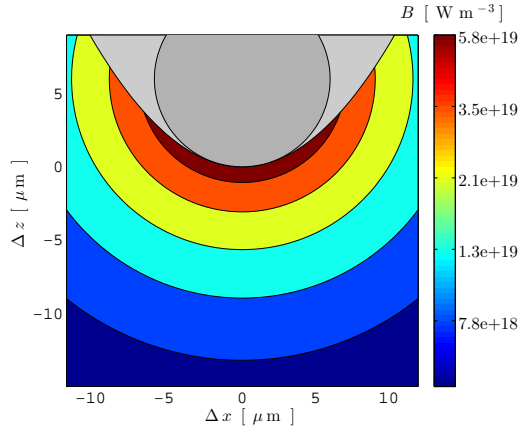
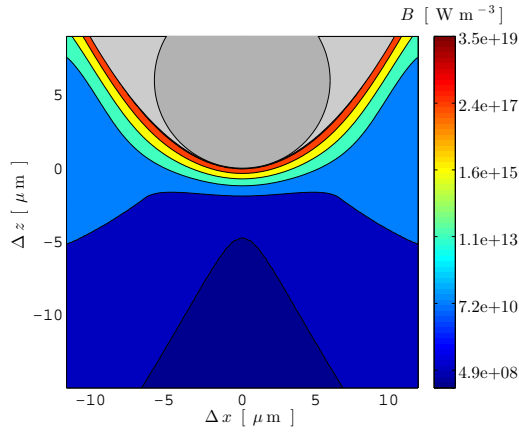
(a) $V_0 = 80$ kV.(b) $V_0 = 240$ kV.

Figure C.10: Spectral radiance B for $\hbar\omega = 6.0$ eV. In fig. 4.7, $V_0 = 120$ kV is plotted. These figures, however, show the effect of changing the voltage. The radiation is not attenuated for the low voltage, and is strongly attenuated for the high voltage. Note the different color scales, these are set to enhance the differences between the figures.

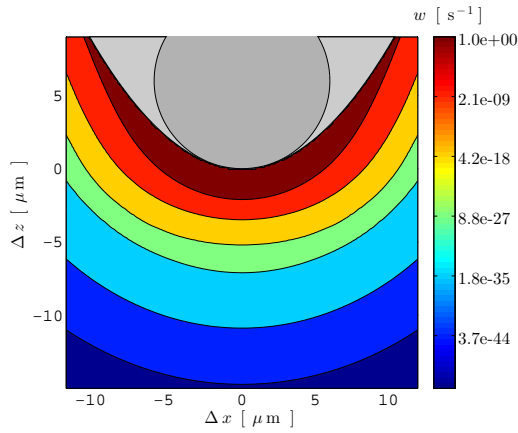


Figure C.11: Ionization rate w for $V_0 = 120\text{ kV}$ and $\sigma_0 = 10^{-21}\text{ m}^2$. In the results, fig. 4.8 is plotted for $\sigma_0 = 10^{-22}\text{ m}^2$. This plot shows that the ionization rate is dominating close to the streamer. The maximum ionization rate on this plot is actually ten times higher than for fig. 4.8, but this is not possible to see on the plot.

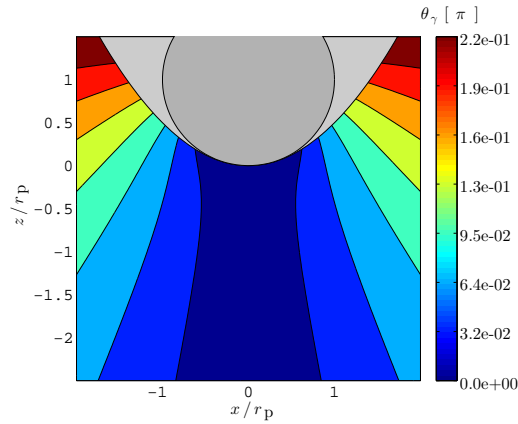


Figure C.12: This is a plot of θ_γ , which is the difference in angle between the photon momentum and the electric field.

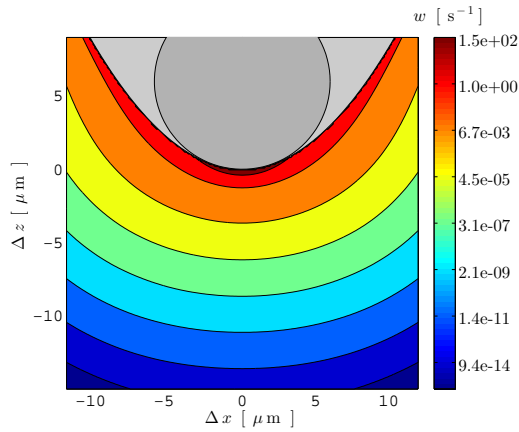
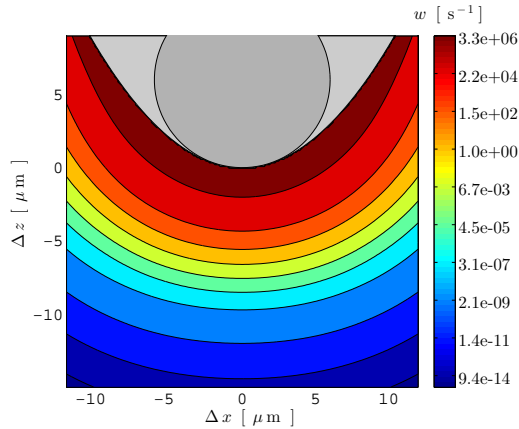
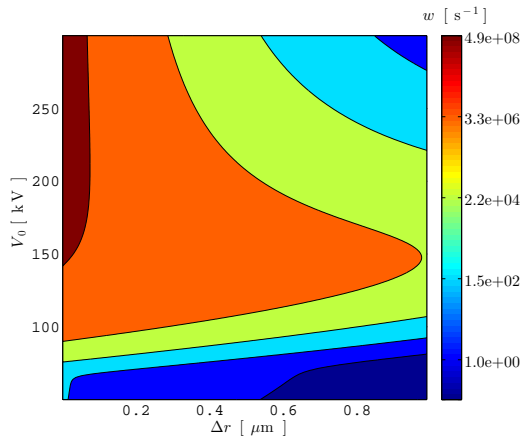
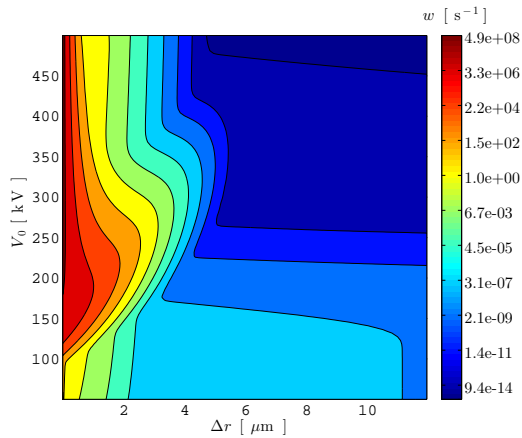
(a) $V_0 = 80 \text{ kV}$, $\sigma_0 = 10^{-22} \text{ m}^2$.(b) $V_0 = 240 \text{ kV}$, $\sigma_0 = 10^{-22} \text{ m}^2$.

Figure C.13: Ionization rate w , variation in voltage V_0 . In the results, fig. 4.8 is plotted for $V_0 = 120 \text{ kV}$. For the low voltage, the radiation peak is not within the bandwidth of the cross section, the result is a low ionization rate. For the high voltage, however, most of the radiation peak is absorbed in close proximity of the needle, resulting in a high ionization rate. Note that the color scales of the figures are different and that the figures are plotted for a small cross section in order to make qualitative trends easier to read.

C.2.3 Voltage range



(a) Close.



(b) Far.

Figure C.14: Ionization rate w , variation in distance Δr . In the results, fig. 4.9 is plotted for $\Delta r = 0 \mu\text{m}$ to $3.0 \mu\text{m}$. These figures gives an impression of how localized the photoionization is occurring. Note the difference in the color scales of the figures.

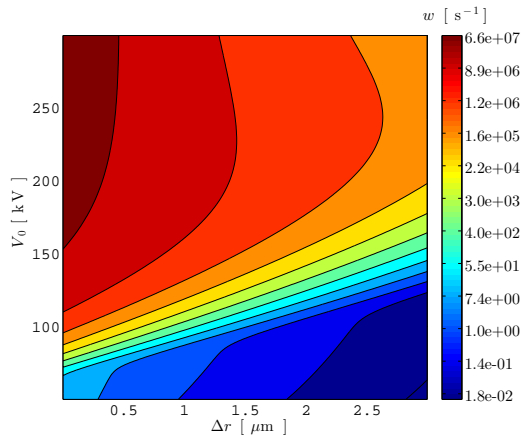
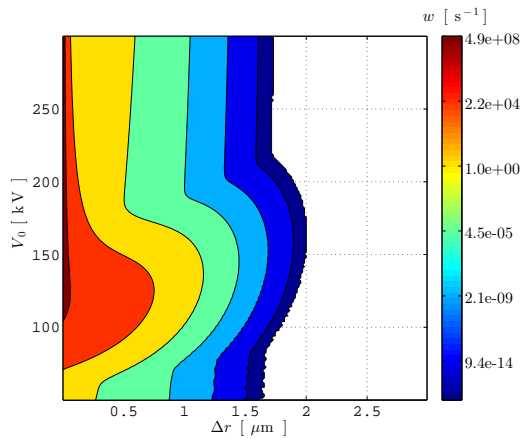
(a) $\sigma_0 = 10^{-22} \text{ m}^2$.(b) $\sigma_0 = 10^{-20} \text{ m}^2$.

Figure C.15: Ionization rate w , variation in σ_0 . In the results, fig. 4.9 is plotted for $\sigma_0 = 10^{-21} \text{ m}^2$. These figures indicate how changing the cross section affects the ionization rate. Increasing the cross section increases the ionization rate, but it also makes it more local. Note the difference in the color scales of the figures.

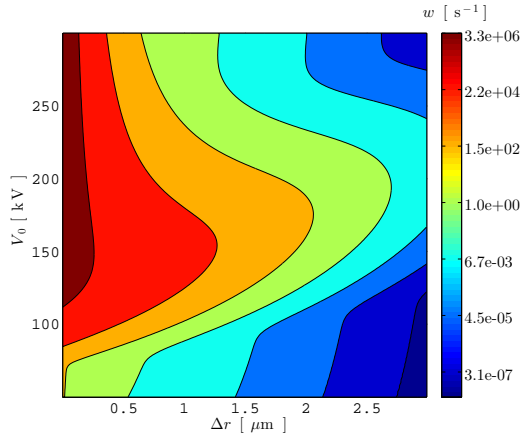
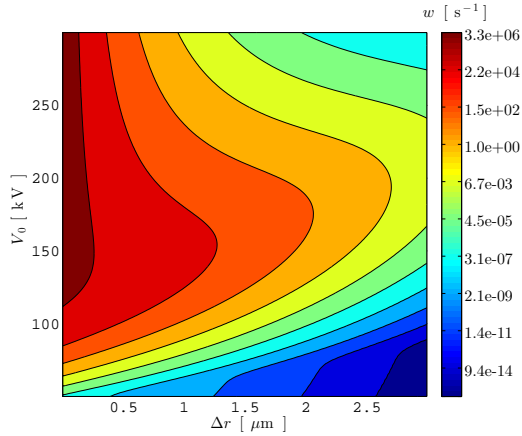
(a) $B_{g0} = 2.5 \times 10^{18} \text{Wm}^{-3}$, $T = 7 \text{kK}$.(b) $B_{g0} = 2.5 \times 10^{18} \text{Wm}^{-3}$, $T = 3 \text{kK}$.

Figure C.16: Ionization rate w , for a lower value of B_{g0} , and variation in the background temperature T . In the results, fig. 4.9 is plotted for $B_{g0} = 8 \times 10^{19} \text{Wm}^{-3}$, $T = 7 \text{kK}$. The effect of the radiation peak in these figures is qualitatively the same on all the figures, changing the magnitude of the peak B_{g0} only changes the maximum ionization rate. These figures does however show that a background radiation at $T = 3 \text{kK}$ has almost no effect on the model. The background radiation at $T = 7 \text{kK}$, however, increases the ionization rate for voltages up to about 90 kV. For higher voltages, the radiation peak dominates the background radiation . Note the difference in the color scales of the figures.

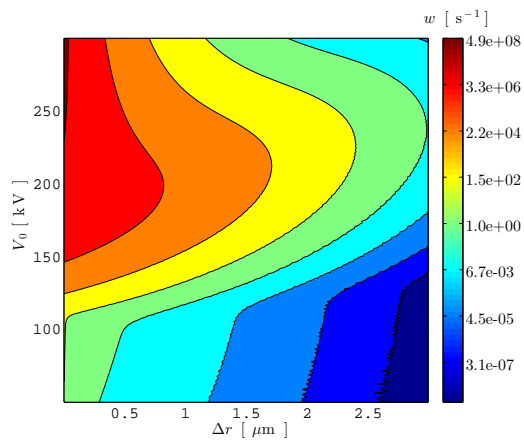


Figure C.17: Ionization rate w , for the angle $\theta = \pi/2$, as a function of voltage V_0 and distance Δr from the streamer head. In the results, fig. 4.9 is plotted for $\theta = \pi$. The plot shows that a higher voltage is required for the radiation peak to cause ionization in this direction.

C.2.4 Movement rate

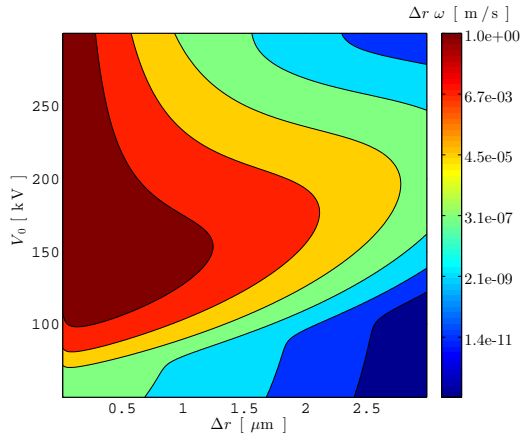
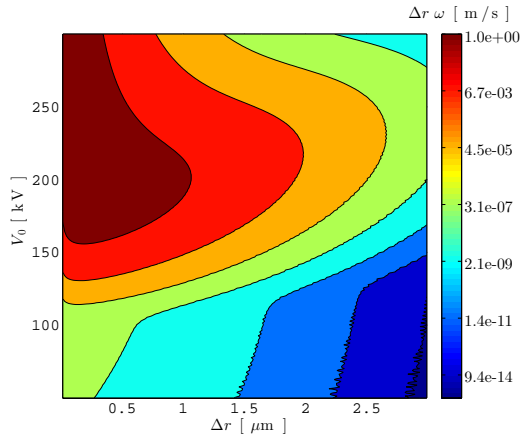
(a) $\theta = \pi$.(b) $\theta = \pi/2$.

Figure C.18: Movement rate $\Delta r w$ as a function of voltage and position. The maximum value of $\Delta r w$ from (a) is plotted in fig. 4.10, and from (b) is plotted in fig. C.20.

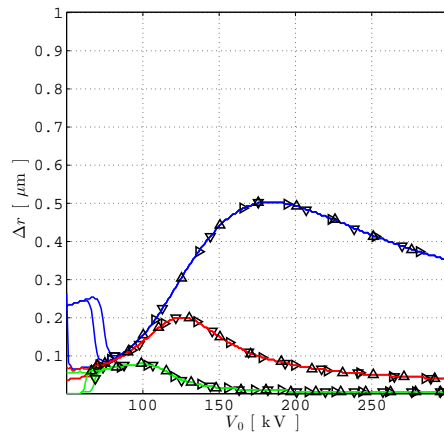
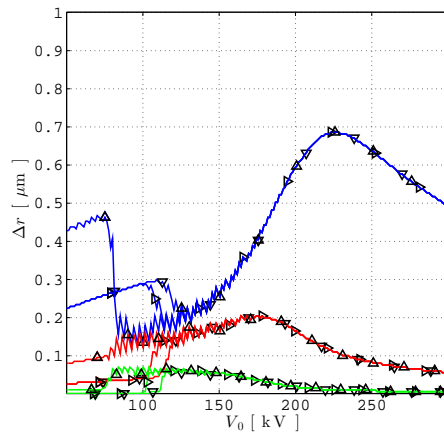
(a) $\theta = \pi$.(b) $\theta = \pi/2$.

Figure C.19: The position from the streamer where the maximum value of $\Delta r w$ is found. These plots are related to the plots in fig. C.18.

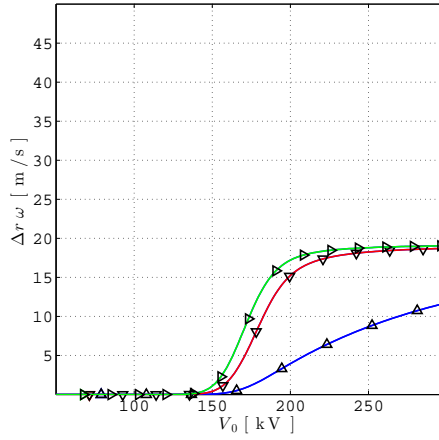


Figure C.20: Maximum movement rate $\Delta r w$ as a function of voltage, for σ_0 equal to 10^{-22} m^2 (Δ), 10^{-21} m^2 (∇), and 10^{-20} m^2 (\triangleright), at $\theta = \pi/2$. The figure is similar to fig. 4.10, but is plotted for another angle θ . The maximum movement rate for this direction is about half of that found for the forward direction.

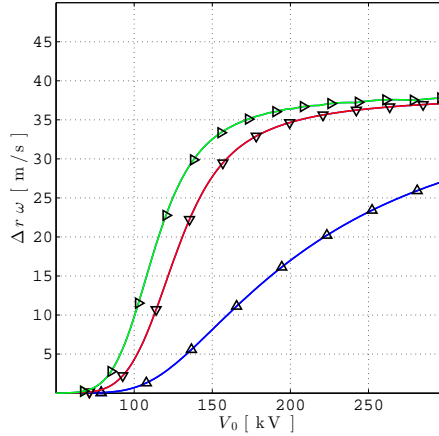


Figure C.21: Maximum movement rate $\Delta r w$ as a function of voltage, for $B_{g0} = 4 \times 10^{19} \text{ Wm}^{-3}$, $\Delta \lambda = 8.0 \text{ nm}$, and σ_0 equal to 10^{-22} m^2 (Δ), 10^{-21} m^2 (∇), and 10^{-20} m^2 (\triangleright). The figure is similar to fig. 4.10, but is plotted for a radiation peak of half the magnitude and twice the width. This results in a wider transition from low to high movement rate.

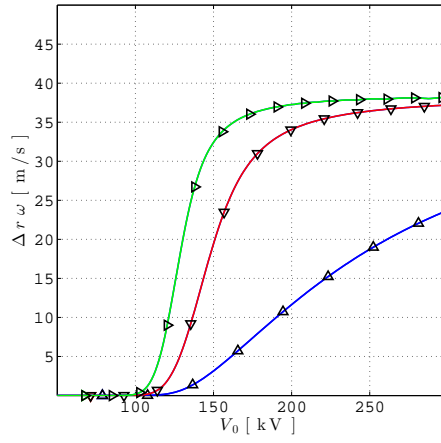


Figure C.22: Maximum movement rate Δr_w as a function of voltage, for $d = 50 \text{ mm}$, and σ_0 equal to 10^{-22} m^2 (Δ), 10^{-21} m^2 (∇), and 10^{-20} m^2 (\triangleright). The gap used here is the same size as LESAINTE AND JUNG¹⁸ used.

Bibliography

1. J. C. Devins. "Breakdown and prebreakdown phenomena in liquids".
In: *Journal of Applied Physics* 52.7 (1981), p. 4531. doi: 10.1063/1.329327
(cit. on p. 1).
2. N. Felici. "Blazing a fiery trail with the hounds (prebreakdown streamers)".
In: *IEEE Transactions on Electrical Insulation* 23.4 (1988), pp. 497–503.
doi: 10.1109/14.7317 (cit. on p. 1).
3. P Gournay and O Lesaint.
"A study of the inception of positive streamers in cyclohexane and pentane".
In: *Journal of Physics D: Applied Physics* 26.11 (1993), pp. 1966–1974.
doi: 10.1088/0022-3727/26/11/019
(cit. on pp. 1, 6, 20, 22, 33, 35–37, 49–51, 63, 76).
4. O Lesaint and P Gournay.
"On the gaseous nature of positive filamentary streamers in hydrocarbon liquids.
I: Influence of the hydrostatic pressure on the propagation".
In: *Journal of Physics D: Applied Physics* 27.10 (Oct. 1994), pp. 2111–2116.
doi: 10.1088/0022-3727/27/10/019 (cit. on pp. 1, 6, 28, 58).
5. P Gournay and O Lesaint.
"On the gaseous nature of positive filamentary streamers in hydrocarbon liquids.
II: Propagation, growth and collapse of gaseous filaments in pentane".
In: *Journal of Physics D: Applied Physics* 27.10 (Oct. 1994), pp. 2117–2127.
doi: 10.1088/0022-3727/27/10/020 (cit. on pp. 1, 34, 58).
6. O. Lesaint and G. Massala. "Positive streamer propagation in large oil gaps:
experimental characterization of propagation modes". In: *IEEE Transactions on
Dielectrics and Electrical Insulation* 5.3 (June 1998), pp. 360–370.
doi: 10.1109/94.689425 (cit. on pp. 1, 6–8, 54).
7. L. Lundgaard, D. Linhjell, G. Berg, and S. Sigmond. "Propagation of positive
and negative streamers in oil with and without pressboard interfaces". In: *IEEE
Transactions on Dielectrics and Electrical Insulation* 5.3 (June 1998), pp. 388–395.
doi: 10.1109/94.689428 (cit. on pp. 1, 2, 25).
8. S Ingebrigtsen, H. Smalø, P.-O. Å strand, and L. Lundgaard.
"Effects of electron-attaching and electron-releasing additives on streamers in
liquid cyclohexane". In: *IEEE Transactions on Dielectrics and Electrical Insulation*
16.6 (Dec. 2009), pp. 1524–1535. doi: 10.1109/TDEI.2009.5361571
(cit. on pp. 1, 13, 20, 22, 28, 36, 49–51, 58, 63, 75).

9. C. Duy, O. Lesaint, A. Denat, and N. Bonifaci.
“Streamer propagation and breakdown in natural ester at high voltage”.
In: *IEEE Transactions on Dielectrics and Electrical Insulation* 16.6 (Dec. 2009),
pp. 1582–1594. doi: 10.1109/TDEI.2009.5361578 (cit. on pp. 1, 6).
10. R Coelho and J Debeau. “Properties of the tip-plane configuration”.
In: *Journal of Physics D: Applied Physics* 4.9 (Sept. 1971), pp. 1266–1280.
doi: 10.1088/0022-3727/4/9/305 (cit. on pp. 2, 18).
11. G. Massala and O. Lesaint. “Positive streamer propagation in large oil gaps:
electrical properties of streamers”. In: *IEEE Transactions on Dielectrics and
Electrical Insulation* 5.3 (June 1998), pp. 371–381. doi: 10.1109/94.689426
(cit. on p. 2).
12. O. L. Hestad, T. Grav, L. E. Lundgaard, S. Ingebrigtsen, M. Unge, and
O. Hjortstam.
“Numerical simulation of positive streamer propagation in cyclohexane”.
In: *2014 IEEE 18th International Conference on Dielectric Liquids (ICDL)*.
IEEE, June 2014, pp. 1–5. doi: 10.1109/ICDL.2014.6893124 (cit. on pp. 3, 20).
13. H. J. Wiesmann and H. R. Zeller.
“A fractal model of dielectric breakdown and prebreakdown in solid dielectrics”.
In: *Journal of Applied Physics* 60.5 (1986), p. 1770. doi: 10.1063/1.337219
(cit. on p. 3).
14. A. L. Kupershtokh and D. I. Karpov.
“Simulation of the development of branching streamer structures in dielectric
liquids with pulsed conductivity of channels”.
In: *Technical Physics Letters* 32.5 (May 2006), pp. 406–409.
doi: 10.1134/S1063785006050129 (cit. on p. 3).
15. M. Kim, R. Hebner, and G. Hallock.
“Modeling the Growth of Streamers During Liquid Breakdown”. In: *IEEE
Transactions on Dielectrics and Electrical Insulation* 15.2 (Apr. 2008), pp. 547–553.
doi: 10.1109/TDEI.2008.4483476 (cit. on p. 3).
16. J. G. Hwang, M. Zahn, and L. a. a. Pettersson. “Mechanisms behind positive
streamers and their distinct propagation modes in transformer oil”. In: *IEEE
Transactions on Dielectrics and Electrical Insulation* 19.1 (Feb. 2012), pp. 162–174.
doi: 10.1109/TDEI.2012.6148515 (cit. on p. 3).
17. J. Jadidian, M. Zahn, N. Lavesson, O. Widlund, and K. Borg.
“Abrupt Changes in Streamer Propagation Velocity Driven by Electron Velocity
Saturation and Microscopic Inhomogeneities”.
In: *IEEE Transactions on Plasma Science* 42.5 (2014), pp. 1216–1223.
doi: 10.1109/TPS.2014.2306197 (cit. on p. 3).
18. O Lesaint and M Jung. “On the relationship between streamer branching and
propagation in liquids: influence of pyrene in cyclohexane”.
In: *Journal of Physics D: Applied Physics* 33.11 (June 2000), pp. 1360–1368.
doi: 10.1088/0022-3727/33/11/315 (cit. on pp. 4, 58, 59, 93).

19. W. An, K. Baumung, and H. Bluhm. "Underwater streamer propagation analyzed from detailed measurements of pressure release". In: *Journal of Applied Physics* 101.5 (2007), p. 053302. doi: 10.1063/1.2437675 (cit. on p. 5).
20. V. M. Atrazhev, V. S. Vorob'ev, I. V. Timoshkin, M. J. Given, and S. J. MacGregor. "Mechanisms of impulse breakdown in liquid: The role of joule heating and formation of gas cavities". In: *IEEE Transactions on Plasma Science* 38.10 PART 1 (2010), pp. 2644–2651. doi: 10.1109/TPS.2010.2046337 (cit. on pp. 8, 49).
21. P. H. Ceccato, O. Guaitella, M. R. Le Gloahec, and A. Rousseau. "Time-resolved nanosecond imaging of the propagation of a corona-like plasma discharge in water at positive applied voltage polarity". In: *Journal of Physics D: Applied Physics* 43.17 (May 2010), p. 175202. doi: 10.1088/0022-3727/43/17/175202 (cit. on p. 8).
22. T. J. Lewis. "A new model for the primary process of electrical breakdown in liquids". In: *IEEE Transactions on Dielectrics and Electrical Insulation* 5.3 (1998), pp. 306–315. doi: 10.1109/94.689419 (cit. on p. 8).
23. E. Ildstad. *TET4160 High Voltage Insulation Materials*. English. 2014 (cit. on p. 9).
24. A. Denat. "High field conduction and prebreakdown phenomena in dielectric liquids". In: *IEEE Transactions on Dielectrics and Electrical Insulation* 13.3 (June 2006), pp. 518–525. doi: 10.1109/TDEI.2006.1657963 (cit. on p. 10).
25. N. Davari, P.-O. Åstrand, S. Ingebrigtsen, and M. Unge. "Excitation energies and ionization potentials at high electric fields for molecules relevant for electrically insulating liquids". In: *Journal of Applied Physics* 113.14 (2013), p. 143707. doi: 10.1063/1.4800118 (cit. on p. 11).
26. H. S. Smalø, O. Hestad, S. Ingebrigtsen, and P.-O. Åstrand. "Field dependence on the molecular ionization potential and excitation energies compared to conductivity models for insulation materials at high electric fields". In: *Journal of Applied Physics* 109.7 (2011), p. 073306. doi: 10.1063/1.3562139 (cit. on p. 11).
27. H. Smalø, P.-O. Åstrand, and S. Ingebrigtsen. "Calculation of ionization potentials and electron affinities for molecules relevant for streamer initiation and propagation". In: *IEEE Transactions on Dielectrics and Electrical Insulation* 17.3 (June 2010), pp. 733–741. doi: 10.1109/TDEI.2010.5492245 (cit. on pp. 11, 33).

28. N. Davari, P.-O. Å strand, M. Unge, L. E. Lundgaard, and D. Linhjell. "Field-dependent molecular ionization and excitation energies: Implications for electrically insulating liquids". In: *AIP Advances* 4.3 (Mar. 2014), p. 037117. doi: 10.1063/1.4869311 (cit. on pp. 11, 12, 33).
29. V. Atrazhev, E. Dmitriev, and I. Iakubov. "The impact ionization and electrical breakdown strength for atomic and molecular liquids". In: *IEEE Transactions on Electrical Insulation* 26.4 (1991), pp. 586–591. doi: 10.1109/14.83675 (cit. on p. 13).
30. M. Haidara and A. Denat. "Electron multiplication in liquid cyclohexane and propane". In: *IEEE Transactions on Electrical Insulation* 26.4 (1991), pp. 592–597. doi: 10.1109/14.83676 (cit. on pp. 13, 49, 50).
31. G. Marr and J. West. *Absolute photoionization cross-section tables for helium, neon, argon, and krypton in the VUV spectral regions*. 1976. doi: 10.1016/0092-640X(76)90015-2 (cit. on p. 14).
32. G. B. Rybicki and A. P. Lightman. *Radiative Processes in Astrophysics*. Wiley, 1979 (cit. on p. 15).
33. E. Merzbacher. *Quantum Mechanics, third edition*. 1998 (cit. on p. 15).
34. J. Lowke and F D'Alessandro. "Onset corona fields and electrical breakdown criteria". In: *Journal of physics D: applied physics* 36.21 (Nov. 2003), pp. 2673–2682. doi: 10.1088/0022-3727/36/21/013 (cit. on p. 22).
35. H. Yamashita, K. Yamazawa, and Y. S. Wang. "The effect of tip curvature on the prebreakdown streamer structure in cyclohexane". In: *IEEE Transactions on Dielectrics and Electrical Insulation* 5.3 (1998), pp. 396–401. doi: 10.1109/94.689429 (cit. on pp. 22, 35–37, 49–51, 63, 77).
36. S Ingebrigtsen, L. E. Lundgaard, and P.-O. Å strand. "Effects of additives on prebreakdown phenomena in liquid cyclohexane: II. Streamer propagation". In: *Journal of Physics D: Applied Physics* 40.18 (Sept. 2007), pp. 5624–5634. doi: 10.1088/0022-3727/40/18/018 (cit. on p. 25).
37. L. Noordam, A. ten Wolde, A Lagendijk, and H. van Linden van den Heuvell. *Time dependence of an atomic electron wave function in an electrical field*. 1989. doi: 10.1103/PhysRevA.40.6999 (cit. on p. 25).
38. S Ingebrigtsen, N Bonifaci, A Denat, and O Lesaint. "Spectral analysis of the light emitted from streamers in chlorinated alkane and alkene liquids". In: *Journal of Physics D: Applied Physics* 41.23 (Dec. 2008), p. 235204. doi: 10.1088/0022-3727/41/23/235204 (cit. on pp. 28, 30, 33).
39. A Denat, N Bonifaci, and M Nur. "Spectral analysis of the light emitted by streamers in hydrocarbon liquids". In: *IEEE Transactions on Dielectrics and Electrical Insulation* 5.3 (June 1998), pp. 382–387. doi: 10.1109/94.689427 (cit. on p. 33).

40. H. Koizumi, K. Shinsaka, and Y. Hatano.
“VUV-optical oscillator strength distributions of molecules and their implications to early events in radiation chemistry”.
In: *International Journal of Radiation Applications and Instrumentation. Part C. Radiation Physics and Chemistry* 34.1 (1989), pp. 87–92.
DOI: 10.1016/1359-0197(89)90012-X (cit. on p. 34).
41. J. M. Jung. “On the photoionisation of liquid cyclohexane, 2,2,4 trimethylpentane and tetramethylsilane”.
In: *Chemical Physics Letters* 380.1-2 (2003), pp. 190–195.
DOI: 10.1016/j.cpllett.2003.08.105 (cit. on pp. 34, 55, 56).
42. T. a. Cool, J. Wang, K. Nakajima, C. a. Taatjes, and A. McIlroy. “Photoionization cross sections for reaction intermediates in hydrocarbon combustion”.
In: *International Journal of Mass Spectrometry* 247.1-3 (2005), pp. 18–27.
DOI: 10.1016/j.ijms.2005.08.018 (cit. on pp. 34, 55).
43. Z. Zhou, L. Zhang, M. Xie, Z. Wang, D. Chen, and F. Qi. “Determination of absolute photoionization cross-sections of alkanes and cyclo-alkanes”.
In: *Rapid Communications in Mass Spectrometry* 24.9 (2010), pp. 1335–1342.
DOI: 10.1002/rcm.4523 (cit. on p. 34).
44. S Ingebrigtsen, L. E. Lundgaard, and P.-O. Åstrand. “Effects of additives on prebreakdown phenomena in liquid cyclohexane: I. Streamer initiation”.
In: *Journal of Physics D: Applied Physics* 40.17 (Sept. 2007), pp. 5161–5169.
DOI: 10.1088/0022-3727/40/17/022 (cit. on p. 50).
45. O. Hestad. “Prebreakdown phenomena in solids and liquids stressed by fast transients: The effect of additives and phase”. PhD thesis. 2010.
ISBN: 9788247124796 (cit. on p. 51).
46. D. Linhjell, S. Ingebrigtsen, L. E. Lundgaard, and M. Unge. “Streamers in long point-plane gaps in cyclohexane with and without additives under step voltage”.
In: *Proceedings - IEEE International Conference on Dielectric Liquids*. 2011.
DOI: 10.1109/ICDL.2011.6015454 (cit. on p. 59).
47. D Linhjell, S Ingebrigtsen, L. E. Lundgaard, and M. Unge.
“Positive Breakdown Streamers and Acceleration in a Small Point-Plane Liquid Gap and Their Variation with Liquid Properties”.
In: *Nordic Insulation Symposium - Nord-IS 13*. 2013 (cit. on p. 59).